Dr. Barbara Ervens
Editor of Atmospheric Chemistry and Physics
NOAA

Dear Barbara,

Listed below are our responses to the comments from Referees #1-3. The referees' comments are in bold type and our responses are in normal font and any changes made to the text of the manuscript are shown in italics. We thank the referees for carefully reading our manuscript and for excellent comments!

Our responses to the referee's comments remain the same as posted in the Interactive Discussion with the exception of our responses to the comments on the refractory black carbon coating analysis. Since we posted our responses to the referee's comments in the Interactive Discussions, we have decided to change our method of determining coating thicknesses. Below we include updated responses to all the referee's comments as well as the reason for switching the method of data analysis. The main conclusions in the paper do not change significantly with the change in the method of determining coating thicknesses.

Sincerely,

Allan Bertram
Professor of Chemistry
University of British Columbia

Anonymous Referee #1

The authors report their case study from two cloud events in southern California. The study involves an impressive number of instruments and methods and shows that refractory black carbon concentrations are consistent with kappa-Köhler theory.

Although carefully done, I am surprised that the manuscript does not express any science questions or hypotheses. It is not clear whether the authors expected that refractory black carbon concentrations do not conform to kappa-Köhler theory. Moreover, the quantification of the coating of the particles (and their activated fraction) is of high value.

Since I am not an expert in the field who knows all unwritten text on the topic, I would have benefited from a standard manuscript that clearly exposes a science question and hypotheses to address these questions. As is, the manuscript is a simple data publication, which has its value, but remains obscure in the aspects how representative the two cloud events are for average or extreme conditions at the site, and what we can learn out of it. The conclusions sound like "nothing new, but now with more accurate numbers". To be acceptable for final publication in ACP I recommend that the authors clearly expose the questions they were asking, what hypotheses they established before carrying out their research, and what was learnt besides having more accurate numbers.

To address the referee's comments, the introduction has been re-written to more clearly outline the objectives of the study. In addition, in the revised manuscript we have tried to better emphasize what was learnt in the current study.

Details:

1) **Somewhere in the methods section or the first reporting of data you must specify what the uncertainty presented after the +/- sign actually is. Is it the standard error of the mean? Or standard deviation from the mean? Or the 95% confidence interval? Or something else? I question the assumption of symmetric uncertainties – please check and report on the distribution of your data and use the appropriate statistical parameter to specify uncertainty. Recall that SE and SD are parameters of the normal distribution and as long as it is not established that the distribution are normal, reporting SE or SD are not the key parameters of your statistics.**

   To address the referee's comments, in the updated manuscript we have specified what the uncertainties represent. Specifically the following changes were made to the updated document:

   a. *pg 11458 line 11: "(1) the five minute averaged CVI counterflow was within ±5σ…" was changed to: "(1) the five minute averaged CVI counterflow*

was within ±6% of the mean counterflow (i.e. ±5σ, where σ is standard deviation)…"

b. pg 11458 lines 15-24: all values reported will be converted to median values and all uncertainties reported will be converted to 10^{th} and 90^{th} percentiles since it was not demonstrated that these data conform to a normal distribution. Furthermore, the following sentence will be added at the end of the paragraph on line 24: *"All values reported in this paragraph are reported as the median and the ranges shown in parenthesis represent the 10^{th} and 90^{th} percentiles."*

c. pg 11462 line 1: The first sentence was changed to: *"The median AF(D_P) for the bulk aerosol and rBC are presented in Fig. 6, where the error bars represent the 10^{th} and 90^{th} percentiles for each 10 nm size bin."*

d. pg 11462 line 12: The first sentence of Section 3.5 was changed to: *"Coating thicknesses were determined using a core and shell Mie model and are shown in Fig. 6c and d, where the error bars represent the 10^{th} and 90^{th} percentiles and the symbols represent the median coating thickness for each size bin."*

2) **Section 2.9: more details on the operation of the FM-100 should be given. See Spiegel et al. (2012) – there are important issues with respect to facing the instrument towards the incoming airstream. Currently the reader has to assume that everything was done correctly, but the details must be given. The FM-100 does not provide the correct number counts by default, and the Mie-scattering correction suggested by Spiegel et al. (2012) is recommended, unless the authors used size bins that are broad enough to state that this does not affect their data. With 20 channels (of 40 that could be used) it appears that the authors probably used equal size bins which were large. But please be more specific on these details.**

To address the referee's comments, the following information on the operation of the FM-100 was added to the updated manuscript:

"A fog monitor (FM-100, model 100, DMT, Boulder, CO), which is a forward scattering optical spectrometer, was located approximately 50 cm above the top of the container, 1 m from the residual inlet, and 1.5 m from the total inlet. The instrument was mounted on a freely rotating board allowing it to be turned into the wind when the wind direction was obvious. Details of the operational theory of the FM-100 can be found in Eugster et al., 2006 and Spiegel et al., 2012. Briefly, ambient droplet laden air is pumped through a wind tunnel and carried to a sizing region where droplets pass a laser beam (wavelength = 658nm). Light that is scattered in the forward direction from a droplet crossing the laser beam is collected by photodetectors and the signals measured are used to assign which size bin within which the droplet falls. From the measured cloud droplet size distribution both the total cloud droplet number concentration (CDNC) and the amount of liquid water content (LWC) present can be determined (Spiegel et al., 2012). The FM-100 used in this study collected droplet counts from droplets with the diameters from 2-50 um using the

manufacture's predefined 20 size bins. The size bin widths using this configuration were 2 um for droplets <20um and 3 um for droplets > 20um. Calibrations of the FM-100 were performed by Droplet measurement Technologies prior to installation."

3) **Turning the FM-100 into the wind direction is very important for Cloud 2 where a +/- 90 degree variability is given on p. 11458, l. 18. It is unclear that this actually means (if it is SD then it basically means that the wind was from all directions, although the mean was from 190 degree), but it must express a very unsteady wind vector during Cloud 2 and hence it is imperative to document proper orientation of the sensor under such conditions.**

   See response to comment #2 above.

4) **11454, 24: correct wording (and work flow) is to fit a function to the data, not to fit the data to a function!**

   The coating analysis method was changed and therefore this wording was removed from the manuscript.

Anonymous Referee #2

The manuscript presents total and cloud-residual aerosol measurements from two cloud events. There is a strong focus on BC aerosol, with interpretation of the ratio of total to cloud-droplet residual concentrations for activated fraction, and of "coating thickness" on BC for consistency with kappa-Koehler theory for CCN activation. This is an interesting "pool to play in", and the observations are interesting; however, more discussion and analysis need to be included to present and support hypotheses about the implications and science to be gleaned from the two case studies included. Two specific areas that need more attention are the SP2 analysis, and inclusion of some discussion about the implicit assumption that BC is involved in the particles that activate as CCN before a droplet forms.

For the SP2 analysis, my concern is focused on two points.

1) **First, the detection efficiency of the SP2 is strongly dependent on laser intensity, the mass of BC in the particles, and, for small BC, the amount of non-BC material internally mixed with BC (Laborde et al., AMT 2012, Atmos. Meas. Tech., 5, 3077–3097, 2012 www.atmosmeas-tech.net/5/3077/2012/doi:10.5194/amt-5-3077-2012).**
   a. **This may be influencing the sharp reduction in apparent BC activated fraction at small sizes (Figure 6). The authors should**

include more information about SP2 laser power, and the level of agreement observed between the SP2s in cloud-free sampling.

The referee raises an important point. As the referee mentioned, the detection efficiency of the SP2 decreases when the diameter of rBC cores become small (i.e. less than approximately 70-90 nm) (Laborde et al., 2012, Schwartz et al 2010).

Since the main conclusions about black carbon in this manuscript are based on relative measurements taken with the two SP2 instruments (i.e. the residual SP2 and the total SP2) the detection sensitivities of the two instruments as a function of size need to be similar. To ensure that this was the case, we carried out the following: First we measured the rBC size distributions with both single particle soot photometers during cloud free sampling conditions and when the CVI was switched off. Since the two instruments gave slightly different results, we applied a size dependent correction factor to the SP2 connected to the total inlet, to bring the two results in agreement. This correction factor has been applied to all the results presented in the initial manuscript. To address the referee's comments, a new figure showing the size dependent correction faction was added to the end of a new figure to the Supplemental Material with the following figure caption:

*"**Fig. S1.** Demonstration of the SP2 size dependent instrument sensitivity correction factor calculation. Panel A shows the number distributions from both the $SP2_{Res}$ (black circles) and the $SP2_{Tot}$ (red squares) each with the corresponding lognormal fits (lines) from ambient cloud-free data; panel B shows the ratio of the $SP2_{Res}$ to the $SP2_{Tot}$, which is used as the correction factor at each size; and panel C shows the distributions after the correction factor has been applied."*

In addition the following text has been added to the updated manuscript:

"It is well known that the detection efficiency of an SP2 decreases when the diameter of rBC cores becomes small (i.e. <~70-90 nm) (Laborde et al., 2012; Schwarz et al., 2010). Since the main conclusions about black carbon in this manuscript are based on relative measurements taken with two SP2s (i.e. the residual SP2 and the total SP2) the detection sensitivities of the two instruments as a function of size need to be similar. To ensure that this was the case, we carried out the following test: We measured the rBC size distributions with both SP2s from side by side ambient sampling of room air during the post-campaign calibration. Since the two instruments gave slightly different results, we applied a size dependent correction factor to the SP2 connected to the total inlet to bring the two results in agreement. Shown in Fig. S1 are rBC size distributions measured during cloud free sampling conditions before the

corrections were applied, the size dependent correction factor applied to the total SP2, and the rBC size distributions measured during cloud free sampling after the correction factors were applied. After applying the correction factors to the total SP2, the two SP2s agreed to within 6% for the total number concentration of rBC particles having diameters between 70 and 220 nm."

b. **Note that cloud processed BC will naturally have thicker coatings than unactivated BC independent of the mechanism by which rBC became associated with the cloud droplets. This potential bias could affect the conclusion about the size distribution of rBC in the cloud residuals compared to total rBC.**

   Here, we think, the referee is pointing out that rBC particles can obtain coatings by in-cloud processes, such as aqueous-phase chemistry. To address the referee's comment, a new section (Sect. 3.7) was added to the revised manuscript where in-cloud aqueous-phase chemistry is discussed.

c. **On another note, the influence of fresh rBC that likely is not thickly coated from the recent city overpass should also be explicitly considered.**

   See response to Comment 3 below.

2) **Secondly, not enough information is given about the potential biases associated with coating thickness determinations for the rBC-containing residual particles; I am concerned that the statement about increasing coating thickness with decreasing rBC core diameter could merely be due to an artifact (although it is expected a priori from our understanding of CCN), and encourage the authors to consider possible bias in their interpretation. At the heart of this issue the point that the SP2 is typically unable to optically size all rBC below an optical size roughly equivalent to that of a 220 nm PSL particle, which I think is roughly equivalent to the optical size of a bare rBC particle of volume equivalent diameter ~160nm. If one only sizes rBC-containing particles with at least this optical size, one will never capture the contribution to coating thickness of small bare or thinly coated rBC masses, but will only size small rBC masses with sufficient internally mixed material to reach this optical size threshold.**

   a. **I suggest that the authors carefully look at and present the statistics of LEO success in different rBC mass ranges to explore this (i.e. in your nomenclature, how what fraction of failed LEO fits is attributed to lack of elastic scattering signal at the 5% of peak laser power point, and how does this fraction change with rBC core mass?). I**

think that you need more analysis to evaluate whether the biases incurred from 50% LEO failure is affecting your interpretation of coating thickness trends.

This referee as well as Referee #3 brings up the issue of potential biases associated with the coating thickness analysis. We thank these referees for bring up this important issue. In the original manuscript coating thicknesses were determined using two avalanche photodiodes (APDs), one of the APDs was a split detector. The split detector APD was used to obtain position information, whereas the APD without the split detector was used to obtain information on the elastic scattering intensity from particles (Gao et al., 2007). The information from the two APDs combined can were used to determine the coating thickness on rBC cores as described by Gao et al., 2007. However, since we submitted our responses to the referee's comments in the interactive discussion, we discovered that in the Soledad studies a large fraction of rBC particles evaporated before the notch position in the split detector, due to poor alignment of the split detector. As a result, position information could not be obtained reliably for a large fraction of the rBC particles. A similar observation has recently been reported (Taylor et al., 2014). Since position information could not be determined reliably for a large fraction of rBC particles, coating thicknesses could not be determined for a large fraction of the rBC particles using the approach described by Gao et al., 2007. As a result we decided to switch our method of extracting coating information. In the updated manuscript, we used the maximum intensity in the elastic scattering signal from the non-split APD detector to determine lower limits to the coating thickness on the rBC particles. A similar approach has been previously used by Subramanian, 2010. Information on the lower limits of the coating thickness is then used to determine the importance of coating thickness, rBC coating volume fraction, and the total diameter (rBC core + 2$\times$coating thickness) on activation of rBC containing particles.

In the revised manuscript we have discussed the effect of the optical detection limits of the SP2 on the new coating analysis. In short, due to the optical detection limits of the non-split detector and due to evaporation of the coatings in the laser beam, the coating thicknesses determined in the revised manuscript are lower limits to the true coating thicknesses.

b. Finally, I don't understand how your failure "b" of scattering at time zero (i.e at the center of the laser beam?) is relevant to the LEO fit. These issues affect figures 6 and 7.

Please see response to Comment #2a from Referee #2.

3) **There needs more discussion of the microphysical route that rBC takes to get incorporated into the cloud droplets. What is the working hypothesis about the interaction?**

Do you believe that BC are internally mixed with other materials in CCN before activation?

a. **What is the coagulation rate for the freshly emitted rBC from the city with existing cloud drops?**

What do these measurements potentially teach us about BC interactions with cloud droplets?

To address the referee's comment we have added a new section (Sect. 3.5) to the revised manuscript where we have discussed the mechanism of incorporating rBC particles into cloud droplets. The text is pasted below:

"Two possible mechanisms exist for incorporating rBC containing particles into cloud droplets: nucleation scavenging and coagulation between the rBC containing particles and cloud droplets. Results and calculations suggest that the dominant mechanism for incorporating rBC particles into the cloud droplets studied was nucleation scavenging. First, the fraction of rBC containing particles activated into cloud droplets increases as the size of the rBC ncreases (see Fig. 6a and b). If coagulation dominated we would expect to see an opposite trend. Second, calculated coagulation rates, together with estimated lifetimes of the cloud droplets cannot explain the fraction of rBC containing particles activated into the cloud droplets, the calculated coagulation rates are too small (see Supplemental Sect. S3)."

4) **How do these results bear on the different approaches to modeling included in the introduction? What is learned from having observed two clouds? The statement that "rBC contributes to CCN" suggests (to me) an active role, what evidence supports this?**

To address the first part of the referee's comment the Introduction of the manuscript has been rewritten and in the revised manuscript we have tried to better emphasize what was learnt in the current study.

To address the second part of the referee's comment please see the response to Referee #2, comment #3.

Specific comments:

5) **Introduction: please clarify the sentence including "we measured BC as a function of size: : :compared to BC as a function of size."**

The introduction was rewritten and therefore the text the referee is referring to was removed.

6) **Section 2.4: Aquadag causes a higher SP2 response per unit mass than ambient rBC. For aquadag calibrations, it is recommended that the Aquadag signal used in the calibration be downward scaled by 0.75 for a better calibration (see Baumgardner et al.: Atmos. Meas. Tech., 5, 1869-1887, 2012 www.atmos-meas-tech.net/5/1869/2012/doi:10.5194/amt-5-1869-2012). It does not appear that this was done here.**

Thank you for pointing this out. To address the referee's comments in the modified document the measured peak heights of the Aquadag calibrations were scaled down by a factor of 0.75 and all calculations for rBC were recalculated with the new calibration equations. In addition, this downward scaling was discussed in the revised manuscript. Specifically, we added the following sentence to the revised manuscript:

"Based on the recommendations by Baumgardner et al., 2012, the average peak heights determined for each of the Aquadag® sizes were scaled downward by 0.75 since Aquadag® has been shown to cause a higher SP2 signal response per unit mass than ambient BC."

7) **Section 2.5: Please explicitly note that the coating thickness has not been validated experimentally, and merely provides consistency between observed optical scattering and mie theory. Of course having noted this, I'll suggest that you extrapolate even further, to coating volume, which is the more relevant quantity for kappa-Koehler.**

To address the first part of the referee's comments we explicitly stated the caveat raised by the referee by including the following sentence to the manuscript:

"It should be noted that the coating thicknesses have not been validated experimentally, but merely provide consistency between the observed optical scattering and Mie Theory."

To address the second part of the referee's comment we have updated and added four new panels to the modified document where we show:

i. The coating volume vs rBC core diameter (Figure 6, panels D and I)
ii. The rBC coating volume fraction vs core diameter (Figure 6, panels E and J).

8) **Non-rBC particles passing through the SP2 can be used to constrain peak position and full width half maximum at times concurrent with the BC observations. These parameters can drift, so I suggest that you check**

variability in this way, and update the parameters on a reasonable time scale if necessary.

Please see response to Comment #2a from Referee #2.

9) **Note that for the SP2 measurement at 1064 nm, there are better estimates for the index of refraction of rBC – see: Method to measure refractive indices of small nonspherical particles: Application to black carbon particle by Nobuhiro Moteki, Yutaka Kondo, Shinichi Nakamura, 2010, in JAS. It is necessary to include the density of the rBC assumed in converting SP2 mass to mie-diameter.**

Thanks very much for binging this to our attention. The coating calculations were redone using a refractive index of 2.26-1.26i and the following text was added to the manuscript:

"The complex index of refraction used for the core was 2.26-1.26i (Moteki et al., 2010b ,Taylor et al., 2014D) and for the shell was 1.5-0.0i, which is consistent with that of dry sulfate or sodium chloride (Metcalf et al., 2012, Schwarz et al., 2008a, Schwarz et al., 2008b)."

10) **Section 2.6: SMPS and SEMS agree to 4% in what? Total count? Count at each size?**

The text in Section 2.6 (pg11456 line 7) of the original manuscript was modified to:

"During cloud free sampling periods the total number concentrations of particles with sizes between 70 and 400 nm measured with the SMPS and SEMS agreed to within 4%"

11) **Section 3.2: +/- 5 sigma does not give the reader much information. Can you present in a more useful was as, e.g. stability in CVI-D50, or % flow?**

Please see the response to Referee #1, comment #1.

12) **Figure 3 does not do a good job in showing the narrated relationship between droplet number and LWC. Perhaps a scatter plot would get this point across more clearly and strongly.**

This is a reasonable suggestion from the Referee. The relationship between droplet number and LWC was only included as a qualitative observation. Since there are no major conclusions drawn from this relationship and since we would prefer to keep the number of plots to a minimum, we would prefer not to include

a new plot to show the relationship between droplet number and LWC, unless the referee strongly objects.

13) **Section 3.3.2: Please comment on the likelihood of droplet condensation on affecting bulk residual size distributions; it is not clear that the CCN that activated have not been affected in the cloud.**

See response to Referee #2, comment #1b.

14) **It is not clear if the residual rBC size distributions have been biased by low laser power/size dependent SP2 detection efficiency. The Detection Efficiency of the Single Particle Soot Photometer (Schwarz et al 2010) discusses these issues. If there is concern about this biasing rBC results, an easy fix is to remove the smallest rBC cores (e.g. below 100 nm or so?) from the analysis.**

Please see the response to Referee #2, comment #1a.

15) **Section 3.5: These results should be examined for possible bias as discussed above.**

Please see the response to Referee #2, comment #1a.

16) **Section 3.6: As the rBC-containing particle size distribution in the ambient is different than that of bulk aerosol, it is not clear to me what Figure 7 is meant to show in terms of the comparison of rBC and bulk aerosol.**

Figure 7 was meant to show the role of total diameter (i.e. rBC core diameter + 2 x coating thickness) in cloud droplet activation. However, since the purpose of including this figure was not clear we have removed it. In replacement, we have added two panels to the original Figure 6, which is now Figure 7, showing the relationship between the total rBC particle diameter (core + 2 $\times$ coating) as a function of the rBC core diameter.

17) **Section 3.7: "rBC cores have thick coatings which lead to overall particle diameters > 100 nm"..This assumes that rBC was present before activation. Please add discuss/support.**

See response to Referee #2, comment #1b and comment#3.

18) **The relevant parameters for kappa-Koehler are the volume and kappa of non-BC material. Figure 9 essentially hides the fact that this is independent of BC content. I suggest explicitly discussing this, and attempting to show**

this in the context of both Figures 7 & 9, by plotting the horizontal axis as a diameter of non-BC materials (i.e. the diameter of only relevant materials for kappa-Koehler theory).

See response to Referee #2 comment #7.

In addition, in Figure 9 a new panel C was added, where Sc was plotted as a function of the volume fraction of the coating at different rBC core diameters and colored by the corresponding kappa values.

Anonymous Referee #3

This MS gives data collected at two out of three cloud events during a field campaign at Mt. Soledad, California. It contains a wealth of data on scavenging of rBC, which could, however, benefit from a more detailed analysis. The authors are very clear about problems experienced during sampling. Actually, the problems that occurred are the usual ones in field studies but are seldom mentioned.

The data are valuable, but the study needs more work and more discussions of implicit and explicit assumptions, as well as a clearer description of the measurement set-up and the measurements themselves. I'll go through the points in the order they appear in the text.
Abstract:

1) **The abstract mentions the total inlet and the CVI (lines 4 and 5), but it is unclear from the abstract alone that the CVI actually is the residual inlet.**

   To make this clearer the abstract (pg 11448 line 4) was changed to:
   "A counterflow virtual impactor (CVI) was used as the inlet to sample cloud residuals while a total inlet was used to sample both cloud residuals and interstitial particles."

2) **Giving percentages of cloud droplets sampled by the CVI without mentioning briefly how total droplet concentrations were obtained is rather confusing.**

   The sentence the referee is referring to has been removed from the abstract in the revised manuscript.

3) **The main results given in the abstract, which are also major results of the study, refer to coating thicknesses of rBC cores of different diameters. The point of coating thickness and core size is one of the most critical ones of the whole study and needs further discussion and investigation (see**

below) could the fact that small rBC cores were found to have thick coatings and large cores thin coatings be an artefact of the upper size cut of the SP2 (220 nm) as larger particles (core+shell) could not be detected?

See response to Referee #2, comment #2a.

4) **section 2.2 inlets:**
Figure 1 is insufficient in its present form. It doesn't show how the droplet residuals were moved to the different instruments - were the particles passed into a sampling manifold where the instruments sampled in parallel or was there a common sampling line with the instruments connected sequentially?

To address the referee's comments Figure 1 was updated to more clearly show how the instruments sampled sequentially. In addition, the following text was added to make it clear how the droplet residuals were moved to the different instruments:

i. pg 11451 line 20: *"The instruments sampling from plenum of the total inlet (Fig. 1) were connected sequentially to a common sampling line (0.25 inch stainless steel tubing). A pump was placed at the end of this sampling line creating a bypass flow of ~2 LPM."*

ii. pg 11452 line 2: *"All instruments sampling downstream of the 3-way valve were sequentially connected to a common sampling line (0.25 inch stainless steel tubing). A pump was place at the end of the sampling line creating a bypass flow of ~2 LPM."*

5) **Where was the FM-100? As percentages of droplets are given: what was the spatial distance between the aerosol inlet(s) and the FM-100?**

See response to Referee #1 comment #2.

6) **How about the homogeniety of the cloud? Patchiness could give a huge effect if the total droplet concentrations and CVI droplet concentrations were not measured at the same spot (and even then patchiness can give problems)**

During this study the FM-100 was located approximately 50 cm above the top of the container, approximately 1 m from the residual inlet, and 1.5 m from the total inlet. This information was added to the revised manuscript to address the referee's comments (see response to Referee #1 comment #2). In addition, Section 3.2 states that data were classified as in-cloud and included for analysis if the five minute averaged LWC was greater than 0.05(g m^{-3}) to remove periods of entrainment, or ``patchy'' regions of the cloud as much as possible (Cozic et al, 2007).

7) **Section 2.4**

   a. **refractory black carbon mass measurements / Section 2.5 coating thickness: how accurate is the calibration with Aquadaq soot? How reliable is the lower cut size of 70 nm? SP2's have their problems, and more discussion of the accuracy of the data is needed.**

   To address the first part of the referee's comments more discussion on the accuracy of the data from the SP2 was included. Specifically, the following sentence was added to the manuscript:

   "The uncertainty in the rBC mass (at the 95% confidence limits) stemming from uncertainty in the fit of the calibration data was 1-16% for $SP2_{Res}$ (depending on particle mass) and 3-25% for $SP2_{Tot}$ (depending on particle mass)"

   To address the second part of the referee's comment, regarding to the lower cut size of 70nm, we believe the referee is referring to the detection efficiency of the SP2.

   Please see the response to Referee #2 comment 1a.

   b. **Same for the measurements of the coating thickness. Why could only 50% of the particles be fitted with the LEO procedure? Please give reasons. This could be a severe limitation of the results of the study.**

   See response to Referee #2, comment #2a.

8) **Section 2.6: which condensation particle counters exactly were used with the SEMS and SMPS?**

   Information on the exact condensation particle counter used with the SEMS was added to the revised manuscript. Specifically, the following was added:

   i. pg 11455 line 28 *"…Hayward, CA) coupled to a condensation particle counter (CPC, model 3781, TSI, St. Paul, MN), which counted…"*

   The SMPS was a model 3034 which is an all in one unit with no manufacturer specified CPC model number.

9) **Section 2.9: this section is much too short. How was the FM-100 operated? Positioning with regard to wind direction? Operation principle (just a short description), calibration, accuracy etc.? This is crucial for the comparison**

with the CVI, especially as the droplet sizes seem to be quite small (and the LWC of cloud 2 very low)

See response to Referee #1 comment #2.

10) **Section 3.3.1: if there is evidence of bimodality in the BulkAero_tot distributions, why perform the size distribution fit only with a single mode lognormal distribution?**

To address the referee's comment, in the revised manuscript we made it clearer why we used a single mode to fit the data. Specifically, the following was added to Section 3.3.1 (pg114459 line 19):

Although their appeared to be at least two overlapping modes in the bulk aerosol size distribution, the shape of the lognormal distribution was rather complicated. Since the conclusions reached from fitting the distributions were minor, we fit the distribution to a single mode lognormal function for simplicity. In the modified manuscript we deleted "both clouds show evidence of at least two overlapping modes" to avoid confusion.

11) **Section 3.3.2 / 3.5: last par. of 3.3.2: most rBC cores are rather near the lower cut size of the SP2. The comparison of the rBC_res and the rBC_tot shows that the droplets contain larger rBC cores than the unactivated aerosol, and that the coating thickness (section 3.5) of larger cores are thinner than those of smaller cores. As the coating thickness could only be determined for the residual inlet, and as the SP2 there had actually a very narrow size range (70 - 220 nm), the result that large particles have thin coatings and small particles have thick ones could be an artefact of the upper cut size of the SP2?**

See response to Referee #2, comment #2a.

12) **If the particles have core-shell structure, of course they are internally mixed, but maybe this should be explicitly stated. Internal mixture can already have occurred in the aerosol entrained into the cloud, and new droplet activation of these particles, as well as through collision of unactivated particles with droplets. Any way to estimate this?**

See response to Referee #2 comment #3.

13) **Section 3.7 / Conclusions There seems to be an impicit assumption that all activated particles have to have diameters > 100nm - why?**

We did not intend to imply that all activated particles have to have diameters > 100nm. We are sorry for the confusion. In order to remove this confusion the following sentences have been changed in the revised:

i. Sorry for the confusion on this point. Our implicit assumption was that uncoated rBC cores with diameters < 100 nm do not get incorporated into the cloud droplets by nucleation scavenging in stratocumulus clouds due to the high supersaturations required for nucleation of uncoated 100 nm rBC particles, and the low critical supersaturations often observed for stratocumulus clouds. To make this assumption more clear we have added the following text to the Conclusions:

"Uncoated rBC cores with diameters < 100 nm are not expected to be incorporated into the cloud droplets sampled at Mt. Soledad due to the due to the high supersaturations required for nucleation uncoated 100 nm rBC particles and the low critical supersaturations often observed for stratocumulus clouds."

14) Do you have meteorology based estimates of the supersaturation history in the clouds (apart from the calculations with kappa-Koehler theory)?

We do not have meteorology based estimates of the supersaturation history, but during the field campaign CCN instruments were connected downstream of the CVI and used to derive upper limits to the cloud supersaturation (Modini et al. 2014, in preparation). The upper limits determined from one of the CCN instrument was 0.1%, which is consistent with the estimated Sc values reported in the current study.

To address the referee's comment the following was added to the revised manuscript in Section 3.7.3 (pg: 11465 line 28):

"During this study a CCN instrument was also connected to the residual inlet and sampled residual particles during cloud events. Data from this instrument were used to derive an upper limit to the cloud supersaturation (Modini, et al, in preparation), and was found to be approximately 0.1%. This upper limit to the cloud supersaturation is consistent with the S_C values reported here using the estimation technique discussed above. "

.

15) Please discuss why are there no large rBC cores with thick coatings? Is this caused by the failure of the LEO fitting procedure? If it is, then this point has to be discussed in depth. The main results are the sizes and

coating thicknesses of rBC incorporated in cloud droplets, and if there are severe limitations to the analysis procedure, the limitations have to be stated at every mention of the results. If it is due to the upper cut size of the SP2, then it should also be stated explicitly

Please see response to Referee #2, comment #2a.

16) Very minor points:

a. section 3.7.1 Crosier (2007) is missing from the list of references

The reference the referee is referring to is Gysel and Crosier (2007). Due to the spacing of the posted discussion article the reference "Gysel and Crosier (2007)" were split over two pages making it appear that there was a reference to just Crosier (2007).

b. section 3.7.3 better use molecular mass instead of molecular weight - it really is a mass and not a weight, even though "weight" is often used.

As suggested, molecular weight was changed to "*molecular mass"* in Section 3.7.3 (pg. 11464 line 25).

Size-resolved observations of refractory black carbon particles in cloud droplets at a marine boundary layer site.

J. C. Schroder[1], S. J. Hanna[1], R. L. Modini[2], A. L. Corrigan[2], S. M. Kreidenweis[6], A. M. Macdonald[3], K. J. Noone[5], L. M. Russell[2], W. R. Leaitch[4], and A.K. Bertram[1]

[1] Department of Chemistry, University of British Columbia, Vancouver, BC, V6T 1Z1, Canada

[2] Scripps Institute of Oceanography, University of California-San Diego, La Jolla, CA, USA

[3] Air Quality Processes Research Section, Environment Canada, Toronto, Ontario, Canada

[4] Climate Chemistry and Measurements Research, Environment Canada, Toronto, Ontario, Canada

[5] Department of Applied Environmental Science, Stockholm University, Stockholm, Sweden

[6] Department of Atmospheric Science, Colorado State University, Fort Collins, CO, USA

Abstract

Size resolved observations of aerosol particles ~~(including black carbon particles)~~ and cloud droplet residuals were studied at a marine boundary layer site (251 m a.m.s.l.) in La Jolla, CA during 2012. A counterflow virtual impactor (CVI) was used as the inlet to sample cloud residuals while a total inlet was used to sample both cloud residuals and interstitial particles. Two cloud events totaling ten hours of in-cloud sampling were analyzed. ~~Since the CVI only sampled cloud droplets larger than ~ 11 µm, less than 100% of the cloud droplets were sampled during the two cloud events (38% of the cloud droplets for the first cloud event and 24% of the cloud droplets for the second cloud). Back trajectories showed that air masses for both cloud events spent at least 96 h over the Pacific Ocean and traveled near, or over populated regions just before sampling.~~ Based on bulk aerosol particle concentrations, mass concentrations of refractory black carbon (rBC) and back trajectories, ~~measured from the total inlet~~ the two air masses sampled were classified as polluted marine air., ~~a classification that was consistent with back trajectory analyses and the mass concentrations of refractory black carbon (rBC) measured from the total inlet. The activated fractions of rBC, estimated from the measurements, ranged from 0.01 to 0.1 for core diameters ranging from 70 to 220 nm.~~ Since the fraction of cloud droplets sampled by the CVI was less than 100 %, the measured activated fractions of rBC should be considered as lower

limits to the total fraction of rBC activated during the two cloud events. Size distributions of rBC and a coating analysis showed that ~~sampled from the residual inlet show that~~ sub-100 nm rBC cores with relatively thick coatings were incorporated into the cloud droplets. ~~in both clouds.~~ For example, 95 nm rBC cores with median coating thicknesses of at least 65 nm were incorporated into the cloud droplets. Measurements also show that the coating volume fraction of rBC cores is relatively large for sub-100 nm rBC cores. For example, the median coating volume fraction of 95 nm rBC cores incorporated into cloud droplets was at least 0.9, a result that is consistent with kappa-Köhler theory. Measurements of the total diameter of the rBC containing particles (rBC core + coating) suggest that the total diameter of rBC containing particles needed to be at least 165 nm to be incorporated into cloud droplets when the core rBC diameter is ≥ 85 nm. This result is consistent with previous work that has shown that particle diameter is important for activation of non-rBC particles. The activated fractions of rBC, determined from the measurements ranged from 0.01 to 0.1 for core rBC diameters ranging from 70 to 220 nm. This type of data is useful for constraining models used for predicting rBC concentrations in the atmosphere. ~~The coating analysis shows that the rBC cores had average coating thicknesses of 75 nm for core diameters of 70 nm and 29 nm for core diameters of 220 nm. The presence of sub-100 nm rBC cores in the cloud residuals is consistent with kappa-Köhler theory and the measured coating thicknesses of the rBC cores.~~

1. Introduction

Black carbon (BC) is a subset of the aerosol population that is emitted as a result of incomplete combustion. Since BC particles strongly absorb solar radiation, they can modify the climate directly. Based on the current best-estimates the BC direct radiative forcing from all present day sources is +0.88 W m^{-2}; however, this the uncertainty associated with this number is approximately 90%. The uncertainty in the BC direct radiative forcing estimates stems from several factors, which include the removal rates of BC from the atmosphere through wet or dry deposition (Bond et al., 2013). BC particles can also potentially act as cloud condensation nuclei (CCN) and contribute to the indirect effects of aerosols on climate (Bond et al., 2013). The current best estimates of the indirect radiative forcing of BC is + 0.23 W m^{-2} (Bond et al., 2013). However, similar to the direct radiative forcing estimate, this indirect radiative forcing estimate is also highly uncertain, with an uncertainty of

approximately 90% (Bond et al., 2013). The uncertainty in the indirect effect radiative forcing estimate is partially due to an uncertainty in BC-cloud interactions (Bond et al., 2013). To better understand the direct and indirect effects of BC on climate, a better understanding of the activation of BC into cloud droplets is needed.

Despite the importance of activation of BC particles into cloud droplets there have only been a small number of studies that have investigated the activation of BC particles into cloud droplets under real atmospheric conditions (see Table 1 in (Cozic et al., 2007)as well as Pratt et al., 2010 and Granat et al., 2010). Of these studies, most have been carried out at mid to high altitude mountain sites (Cozic et al., 2007; Hitzenberger et al., 2000, 2001; Kasper-Giebl et al., 2000; Sellegri et al., 2003). Only a few studies have investigated the activation of BC particles at a marine or coastal site (Gieray et al., 1997; Granat et al., 2010). In addition, almost all of the previous studies have focused on the fraction of total BC mass activated into cloud droplets. For example, (Hallberg et al., 1992) measured the mass scavenging of BC into fog droplets at a polluted site in the Po Valley (Italy). They found that the mass fraction of scavenged BC (0.06) was statistically smaller than the scavenged fraction of sulphate (0.18). Similar results were obtained when sampling stratocumulus clouds at a mountaintop site at Kleiner Feldberg Germany. There a statistically significant difference in scavenging was also observed; the scavenged fraction of sulphate at this site was 0.52 while the scavenged fraction of BC was 0.15 (Hallberg et al., 1994). In this latter case, observations showed that BC particles found as cloud droplet residuals were of mixed composition, often having a water-soluble component that varied as a function of size. These studies are not able to determine the relative contribution of particle size and composition to the activation of BC into clouds. Although, the fraction of total BC mass activated is useful for validating models, the CCN properties of rBC containing particles are more closely linked to number and particle size.

Recent studies have compared concentrations of BC particles measured over the central Pacific from 85^{o}N to 67^{o}S during the HIAPER (High-Performance Instrumented Airborne Platform for Environmental Research) Pole-to-Pole Observations (HIPPO) campaign, with predictions using a global chemical transport model (Wang et al., 2014). The authors concluded that most models may not be accurately simulating the scavenging of BC particles into cloud droplets (Wang et al., 2014). To help better constrain these models, additional studies on the activation of BC into cloud droplets under real atmospheric conditions and at

different locations and times would be helpful.

The single particle soot photometer (SP2) is an instrument recently developed to determine the refractory black carbon (rBC) mass of individual particles. With this instrument, size distributions of rBC can be obtained in real time. In addition, this instrument provides information on coating thicknesses of the rBC containing particles. The SP2 has now been used extensively to determine the size distribution and coating thicknesses of rBC particles in the atmosphere. Here, we apply this technique to investigate the activation of rBC particles in stratocumulus clouds at a marine boundary layer site. Specific questions to be addressed include the following: (1) what is the activated fraction of rBC as a function of particle size in the marine stratocumulus clouds studied? (2) Do small (sub-100 nm) rBC cores get incorporated into the cloud droplets? (3) What is the thickness of the coating on the rBC cores that are incorporated into the cloud droplets? (4) Is the rBC coating volume fraction and the total diameter (rBC core + coating thickness) important for activation of rBC into cloud droplets? (5) Are the results consistent with kappa-Köhler theory, which is used in advanced modelling studies to describe the activation of rBC particles into cloud droplets (e.g. (Fierce et al., 2013; Riemer et al., 2010)).

~~Black carbon (BC) particles, which typically have sizes less than 1 μ m, are emitted into the atmosphere through incomplete combustion of fossil fuels or biomass burning (Bond et al., 2013). When first emitted into the atmosphere these particles are thought to mainly be hydrophobic. During their atmospheric lifecycle hydrophilic substances, such as sulfate or water soluble organics, can form a coating surrounding the black carbon cores (Ching et al., 2012; Met- calf et al., 2012; Schwarz et al., 2008b), enabling the particles to act as cloud condensation nuclei (CCN). Modeling studies have shown that this process can occur in the boundary layer on the order of hours during the daytime (Riemer et al., 2004, 2010).~~

~~By absorbing solar radiation or by acting as CCN, BC particles can influence climate both directly and indirectly (Bond et al., 2013; Wang, 2013; Wang et al., 2013; Zhuang et al., 2010). To predict both the direct and indirect effects of black carbon on climate, a good understanding of the CCN ability of BC is needed (Koch et al., 2011; Vignati et al., 2010; Wang, 2013). When de- scribing the CCN properties of black carbon in atmospheric models, different approaches have been applied. Often BC is initially assumed to be CCN inactive and converted to a CCN active species after a prescribed time and at a constant efficiency (Koch et~~

al., 2011; Vignati et al., 2010; Wang, 2013). Alternatively, the CCN properties of particles containing BC in models have been described by Kohler theory (Ching et al., 2012; Jacobson, 2012; Koch et al., 2011; Riemer et al., 2010).

The CCN ability of BC particles has been studied in both laboratory and field studies (Cozic et al., 2007; Dusek et al., 2011; Hallberg et al., 1992, 1994; Henning et al., 2010, 2012; Hitzenberger et al., 2000, 2001; Kasper-Giebl et al., 2000; Koehler et al., 2009; Kuwata et al., 2009; Noone et al., 1992; Petters et al., 2009; Petzold et al., 2005; Popovicheva et al., 2011; Sellegri et al., 2003;
Verheggen et al., 2007). Laboratory studies have examined both coated and uncoated black carbon particles (Dusek et al., 2011; Henning et al., 2010, 2012; Koehler et al., 2009; Petters et al., 2009; Petzold et al., 2005; Popovicheva et al., 2011). These studies have shown that for uncoated flame or spark-generated BC the particles are not activated into cloud droplets even with supersaturations of ≥ 1 % (Henning et al., 2012). On the other hand, once BC is coated with hygroscopic material the supersaturation required for activation is significantly decreased, a decrease that can be described under laboratory conditions by
Kohler theory (Henning et al., 2010, 2012; Petzold et al., 2005; Popovicheva et al., 2011).
Field measurements of the activated fraction of BC in cloud droplets have also investigated the CCN ability of BC particles. Most measurements have shown that as BC particles age in the atmosphere the fraction incorporated into cloud droplets increases (Cozic et al., 2007; Hitzenberger et al., 2000, 2001; Kasper-Giebl et al., 2000; Sellegri et al., 2003; Verheggen et al., 2007). An exception to this trend is the work done by Granat et al. (2010) which showed that after several days of travel in the winter subtropical marine environment, soot retained much of its hydrophobic properties. However, the conclusions stated in this study assume that hygroscopicity controlled the removal of BC through wet scavenging, when a more important factor is particle size. Furthermore, the washout ratio, which is the metric used to interpolate scavenging efficiencies, was computed for BC mass and not number. Therefore, direct comparisons of their work and the work presented here are difficult to make. Some field studies (Hallberg et al., 1992, 1994) have shown that 10–20 % of atmospheric BC can activate at supersaturations of between ≈0.2–0.5 %.

Although the activated fraction of BC in cloud droplets have been measured at some locations, the true contribution of BC to CCN in the atmosphere is unknown, yet potentially

~~significant (Chen et al., 2010). Measurements of the activated fraction of BC as a function of size are important to test our current understanding of the incorporation of BC particles into cloud droplets. In this study the size resolved activated fractions of rBC and the totala aerosol were investigated at a marine boundary layer site (251m a.m.s.l) in La Jolla, CA. Coating thicknesses of BC cores in the cloud residuals were also determined. The measurements of BC as a function of size in cloud residuals were further compared to predictions with kappa-Kohler theory.~~

2. Site, sampling and analysis

2.1. Site description

The sampling site was located below the peak of Mt. Soledad (251 m a.m.s.l.) which is ~~3~~ ~ 2 km off the coast of the Pacific Ocean in La Jolla, CA (32.8400° N, 117.2769° W) with mostly light commercial and residential activities in the area. The city of La Jolla is predominately residential with a population of approximately 43,000 people and is situated 24 km north of San Diego (population 1.3 million), the closest urban center (Zhao et al., 2014). The cloud periods occurred primarily at night when these activities are at a minimum.

Data was collected from 27 May to 18 June 2012 using instruments housed in a modified shipping container. A total of three stratocumulus cloud~~s~~ events were sampled during this time frame. The first cloud event was ~~rejected~~ excluded from this analysis due to an instrumental error. The second cloud event occurred from 12 June 2012 20:43 to 13 June 2012 11:35 PDT, and hereinafter called Cloud 2. The third cloud event took place from 17 June 2012 20:36 to 18 June 2012 07:52 PDT, and called Cloud 3 for the remainder of the document.

2.2. Inlets

Two inlets, referred to as the total inlet and residual inlet, were used during this study (Fig. 1). The total inlet measured both interstitial and cloud residual particles during cloud events. This heated inlet was designed and built following the specifications reported by Bates et al. (2002) and therefore assumed to have the same transmission efficiency, namely > 95% for particles less than 6.5 μm, using a ~900 LPM bypass flow. The instruments sampling from the plenum of the total inlet (Fig.1) were connected sequentially to a common sampling line (0.25 inch stainless steel

tubing). A pump was placed at the end of this sampling line creating a bypass flow of ~2 LPM.

The intake of the residual inlet was a counterflow virtual impactor (~~CVI,~~ see Sect. 2.3 and ~~Appendix A~~Supplementary Material Sect.S1) that enabled the sampling of cloud droplets without contamination from interstitial particles, or ambient gases, thus only the residual particles of the cloud droplets were sampled. This inlet was used only during cloudy periods and was connected to a branch of the total inlet by a 3-way valve (Fig.1). During a cloud event, the valve was manually switched so that cloud droplets were sampled through the counterflow virtual impactor (CVI) and cloud residuals were measured by instrumentation connected downstream of the valve. At times when no clouds were present the valve was switched such that all instruments were sampling ambient particles. All instruments downstream of the 3-way valve were sequentially connected to a common sampling line (0.25 inch stainless steel tubing). A pump was also placed at the end of the sampling line creating a bypass flow of ~2 LPM.

Since much of the analysis used in this paper is based on a measured ratio of particle number concentrations it was necessary to ensure that there were no significant losses of particles due to the inlet configurations. Therefore, particle losses from diffusion, sedimentation, turbulent inertial deposition and inertial deposition from both bends and contractions for the total and residual inlets (assuming cloud free sampling) were calculated using the Particle Loss Calculator (Von der Weiden et al., 2009) and found to be < 2% for particles with diameters between 0.07 and 1 μm, covering the size range used for this analysis.

2.3. Counterflow virtual impactor sampling

The CVI was based on the design of Noone et al., 1988., where droplet laden air was drawn into the CVI using a high velocity air intake vacuum ($\approx 92\ m\ s^{-1}$). Only those droplets with enough inertia to overcome a counterflow of zero air with an average flow rate of ≈ 5 LPM made it past the region known as the stagnation plane and were ~~therefore~~ entrained into the sample flow and transported to the instruments downstream. Water from these droplets began evaporating upon impact with the warm dry counterflow air, held at a constant temperature of 40 °C, and particles were further dried by a heated section of the sampling tube, also at 40 °C, leaving only the droplet residuals to be sampled downstream. If the droplets were completely evaporated, any volatile gases in the cloud droplets, such as nitric acid, likely evaporated and were not part of the

residual particles (Zhao et al., 2014) . If some water was retained by the residual particles at this temperature, a fraction of highly soluble volatile components may have also remained.

The smallest droplet diameter for which 50% of the droplets are sampled is considered to be the CVI cut-size (CVI-D_{50}) and is the diameter for which a droplet's stopping distance is greater than the CVI inlet diameter and the length to the end of the stagnation plane (Anderson et al., 1993; Noone et al., 1988). For the clouds sampled in this study a CVI-D_{50} of 11.5 ± 0.7 µm and 11.6 ± 0.7 µm for Cloud 2 and Cloud 3, respectively, were calculated (see ~~Appendix A~~Supplementary Material Sect. S1 for details).

Due to the properties of a CVI, particle concentrations are enhanced at the exit of the CVI compared to ambient conditions. Enhancement factors (EF) of 7.1 and 7.4 for Cloud 2 and Cloud 3, respectively, were calculated based on the flow rates used during sampling (see ~~Appendix A~~Supplementary Material Sect. S1).

2.4. Black carbon measurements

Refractory black carbon (rBC) was measured from the total inlet and the residual inlet using two separate single particle soot photometers (SP2, DMT, Boulder, CO). These instruments are referred to as the total SP2 ($SP2_{Tot}$) and the residual SP2 ($SP2_{Res}$). The location of these instruments is shown in Fig.1. The SP2 has been described in detail elsewhere (Moteki and Kondo, 2007; Schwarz et al., 2006; Stephens et al., 2003). Briefly, particles are sampled at ≈ 0.12 LPM and carried directly into a chamber housing a high intensity (≈ 1 MW cm^{-2}) intra-cavity Nd:YAG laser operating at $\lambda = 1064$ nm. BC particles are rapidly heated, through absorption, to incandescence, where the emitted visible light is detected by two photomultipliers. The mass of individual rBC particles can be determined using a calibration plot, where the amplitude of the detector response is proportional to the mass of a reference material. The two SP2s used in this study were calibrated pre and post-campaign with Aquadag ® (Moteki et al., 2009), using effective densities reported by Gysel et al., 2011. Based on the recommendations by Baumgardner et al., 2012, the average peak heights determined for each of the Aquadag® sizes were scaled downward by 0.75 since Aquadag® has been shown to cause a higher SP2 signal response per unit mass than ambient BC.

The calibration parameters used to determine mass were taken from a ~~second order polynomial~~linear fit of the combined pre and post-campaign data. The uncertainty in the rBC mass (at the 95% confidence limit) stemming from uncertainty in the fit of the calibration was 1-16% for $SP2_{Res}$ (depending on particle mass) and 3-25% for $SP2_{Tot}$ (depending on particle mass). A volume equivalent diameter was also determined from the measured mass assuming a black carbon density of 1.8 g cm^{-3} (Bond and Bergstrom, 2006). The $SP2_{Res}$ was a 4 channel instrument with a detection range of approximately 70 to 220 nm, whereas the $SP2_{Tot}$ was an 8 channel instrument with a detection range of 70 to 558 nm.

It is well known that the detection efficiency of an SP2 decreases when the diameter of rBC cores becomes small (i.e. <~70-90 nm) (Laborde et al., 2012; Schwarz et al., 2010). Since the main conclusions about black carbon in this manuscript are based on relative measurements taken with two SP2s (i.e. the residual SP2 and the total SP2) the detection sensitivities of the two instruments as a function of size need to be similar. To ensure that this was the case, we carried out the following test: We measured the rBC size distributions with both SP2s from side by side ambient sampling of room air during the post-campaign calibration. Since the two instruments gave slightly different results, we applied a size dependent correction factor to the SP2 connected to the total inlet to bring the two results in agreement. Shown in Fig. S1 are rBC size distributions measured during cloud free sampling conditions before the corrections were applied, the size dependent correction factor applied to the total SP2, and the rBC size distributions measured during cloud free sampling after the correction factors were applied. After applying the correction factors to the total SP2, the two SP2s agreed to within 6% for the total number concentration of rBC particles having diameters between 70 and 220 nm.

2.5. Refractory black carbon coating thickness measurements

In addition to measuring the incandescence signal, the SP2 ~~measured~~measures the elastically scattered light from rBC and non-rBC containing particles with two avalanche photodiodes (APDs). Both APDs were set to the high gain setting for collection, and one of the APDs was a split detector. The APDs generate a time dependent signal as particles pass through the Gaussian laser beam. The split detector APD ~~is~~ can be used to obtain position information, whereas the APD without the split detector is used to obtain information on the elastic scattering intensity from particles (Gao et al., 2007). The information from the two APDs

combined can be used to determine the coating thickness on rBC cores as described by Gao et al., 2007. However, in the Soledad studies a large fraction of rBC particles evaporated before the notch position in the split detector, due to poor alignment of the split detector. As a result, position information could not be obtained reliably for a large fraction of the rBC particles. A similar observation has previously been reported (Taylor et al., 2014). Since position information could not be determined reliably for a large fraction of rBC particles, coating thicknesses were not determined using the approach described by Gao et al., 2007. Instead, we used the maximum intensity in the elastic scattering signal from the non-split APD detector to determine lower limits to the coating thickness on the rBC particles. A similar approach has been previously used (Subramanian et al., 2010). This coating analysis was only performed on the data from the residual SP2. In other words, we only extracted coating information for rBC containing particles sampled from the residual inlet. When a rBC containing particle intersects with the laser beam the particles are heated, and any coating material can evaporate. As a result, the maximum elastic scattering signal measured with the non-split APD detector may not represent the original size of the coated rBC particle. Because of the evaporation process, the maximum intensity from the non-split APD detector only provides a lower limit to the coating thicknesses of rBC containing particles (Gao et al., 2007; Subramanian et al., 2010).

The signal from the non-split detector was calibrated using polystyrene latex (PSL) beads ~~(PSL) particles~~ (200 and 300 nm in diameter). This gives a calibration curve that relates the amplitude of the measured scattering signal to the scattering intensity determined from ~~a~~ Mie calculations. These Mie calculations involved calculating the scattering intensity for each PSL size over the solid angle of the SP2 detector (a full-angle cone of 65^{o} at 45^{o} and 135^{o} from the laser axis (Gao et al., 2007; Schwarz et al., 2008b) using a Mie code (Leinonen) based on that of (Mätzler, 2002a, 2002b). The refractive index used for the PSL Mie calculations was 1.59-0.0i.

~~The information from the two APDs was used to determine the coating thicknesses on rBC cores as described by (Gao et al., 2007). Due to a failure of the split detector on the SP2 connected to the total inlet, coating thicknesses on rBC cores were only determined from the data collected with the SP2 connected to the residual inlet. To determine coating thicknesses the scattering amplitudes for rBC containing particles were determined using the leading edge only (LEO)~~

~~fitting method (Gao et al., 2007). In short, the early part of the elastic scattering signal (up to 5% of the maximum laser intensity (Gao et al., 2007) was fit to a Gaussian function and the maximum scattering amplitude was retrieved from the fit. Parameters included in the curve fitting were the peak position and full width at half maximum, determined with the positional information from the split detector and calibration measurements with PSL particles prior to the field campaign.~~

Since the mass of the rBC core is known from the incandescence signal and the ~~maximum~~ scattering amplitude is ~~determined from the leading edge analysis~~known from the non-split APD detector, a core-shell Mie model can be employed to determine what coating thickness would give the measured scattering signal for that particular particle (Gao et al., 2007; Schwarz et al., 2008b).In this work a core-shell Mie model was used to construct a lookup table for core diameters of 60 to 220 nm (in 1 nm increments) and shell thicknesses from 0 to 360 nm (in 1 nm increments). The complex index of refraction used for the core was ~~1.95-0.79i (Bond et al., 2006)~~2.26-1.26i (Moteki et al., 2010; Taylor et al., 2014) and for the shell was 1.5-0.0i, which is consistent with that of dry sulfate or sodium chloride (Metcalf et al., 2012; Schwarz et al., 2008a, 2008b). The PSL calibration was used to scale all calculated values to measured values. The elastic scattering amplitudes and the rBC core diameters were then used with this lookup table to determine lower limits to the coating thicknesses for each rBC containing particle. It should be noted that the coating thicknesses have not been validated experimentally, but merely provide consistency between the observed optical scattering and Mie theory.

For small particles, although the incandescence measurements can size rBC cores down to ~70nm, the SP2 elastic scattering optical detection limit means that scattering from bare rBC cores below ~110 nm cannot be measured. As particle size decreases below 110 nm, thicker and thicker coatings are required to produce a measureable scattering signal. In this analysis any particle with no measureable scattering signal was assumed to have a coating thickness of 0 (i.e. they were assumed to be bare rBC cores), even though they may actually have had a thin coating. This also leads to a lower limit for coating thicknesses for particles below ~110 nm. The fraction of particles with no detectable scattering was 33% for Cloud 2 and 17% for Cloud 3.

For large rBC cores the optical detector became saturated when even relatively modest coatings are present. For example, the scattering from a 220 nm rBC core with a coating

thickness of 40 nm would saturate the SP2 optical detector. In this analysis, the coatings for particles with saturated scattering signals were calculated using the saturation limit of the detector, again resulting in a lower limit for coating thickness. The fraction of particles with saturated scattering signals was 6% for cloud event 2 and 4% for cloud event 3.

In summary, due to the optical detection limits of the non-split detector and due to evaporation of the coatings in the laser beam, the coating thicknesses determined in this work, are lower limits to the true coating thicknesses.

~~As mentioned above, only data collected with the SP2 connected to the residual inlet was analyzed for coating thickness. Approximately 99% of the rBC containing particles detected with the $SP2_{Res}$ had elastic scattering signals above the background signals on the APDs. Nevertheless, only 50% of the rBC containing particles detected with the $SP2_{Res}$ were successfully fit with the LEO fitting procedure. Hence, coating information reported here is only from a subset of the rBC particles measured with the $SP2_{Res}$. Failure to fit the elastic scattering signals with the LEO procedure was mainly due to either; a) large scattering signals that saturated the APD detector, or b) time dependent scattering signals were above 5% of the maximum laser intensity at time zero. 11% and 27% of all rBC containing particles detected with the $SP2_{Res}$ had a failure due to a) and b), respectively.~~

2.6. Size distribution measurements of the bulk aerosol

Two instruments were used to measure size distributions of the bulk aerosol (see Fig.1). Size distributions of the bulk aerosol sampled from the total inlet were determined with a scanning electrical mobility spectrometer (SEMS, model 2002, BMI, Hayward, CA) coupled to a condensation particle counter (CPC, model 3781, TSI, St. Paul, MN), which counted particles into 61 discrete size bins from 0.01-1 μm with a 5 min scan time interval. Size distributions of bulk aerosol, sampled from the residual inlet, were determined with a scanning mobility particle sizer (SMPS, model 3034, TSI, St. Paul, MN), which recorded particle counts into 55 size bins from 10-487 nm with a 3 min scan time interval. Both the SEMS and SMPS operate based on the coupling of a size selecting differential mobility analyzer and a condensational growth particle counter. During cloud free sampling periods the total number concentration of particles

between 70 and 400 nm measured with the SMPS and SEMS agreed to within 4%.

2.7. Aerosol mass spectrometry

To characterize the chemical composition of the cloud droplet residuals an online aerosol mass spectrometer (HR-ToF-AMS, Aerodyne Research Inc., Billerica, MA) was operated downstream of the CVI on theresidual inlet. The HR-ToF-AMS measures non-refractory, sub-micrometer aerosol chemical composition at high time resolution (DeCarlo et al., 2006). Here we only consider data measured by the HR-ToF-AMS in its mass-spectrum and V-modes of operation. These data were recorded as 2 minute averages every 4 – 6 minutes, depending on how many other modes of operation (W-mode, light scattering) the instrument was alternating between. Size-resolved composition data for the residual particles measured by the HR-ToF-AMS in time-of-flight mode are not considered here since the signal was generally at or below the detection limit. Standard quantification procedures (Allan et al., 2004) were applied to the mass spectra measured by the HR-ToF-AMS to determine the relative concentrations of the non-refractory species (organic, nitrate, sulfate, ammonium and chloride) typically reported by aerosol mass spectrometry.

2.8. Back trajectories

Air mass back trajectories were calculated using the NOAA Hybrid Single Particle Lagrangian Integrated Trajectory Model (HYSPLIT) (Draxler and Rolph, 2013; Rolph, 2013). All trajectory calculations used the National Centers for Environmental Predictions EDAS meteorological dataset. Trajectories were calculated starting at 10m a.g.l., 96 h backwards in time, and at hourly intervals throughout the entire period of cloud sampling.

2.9. Cloud properties

A fog monitor (FM-100, model 100, DMT, Boulder, CO), which is a forward scattering optical spectrometer, was ~~stationed~~ located approximately 50 cm above the top of the container, 1 m from the residual inlet, and 1.5 m from the total inlet. The instrument was mounted on a freely rotating board allowing it to be turned into the wind when the wind direction was obvious.~~on top of the container providing an in-situ measurement of the cloud droplet number concentration (CDNC) in twenty discrete size bins ranging from 2-50 µm, whilst~~

~~simultaneously monitoring the liquid water content (LWC) present with a 1 second time resolution (Eugster et al., 2006).~~ Details of the operational theory of the FM-100 can be found in Eugster et al., 2006 and Spiegel et al., 2012. Briefly, ambient droplet laden air is pumped through a wind tunnel and carried to a sizing region where droplets pass a laser beam (wavelength = 658nm). Light that is scattered in the forward direction from a droplet crossing the laser beam is collected by photodetectors and the signals measured are used to assign which size bin within which the droplet falls. From the measured cloud droplet size distribution both the total cloud droplet number concentration (CDNC) and the amount of liquid water content (LWC) present can be determined (Spiegel et al., 2012). The FM-100 used in this study collected droplet counts from droplets with the diameters from 2-50 um using the manufacture's predefined 20 size bins. The size bin widths using this configuration were 2 um for droplets <20um and 3 um for droplets > 20um. Calibrations of the FM-100 were performed by Droplet measurement Technologies prior to installation.

3. Results and discussion

3.1. Back trajectories

The back trajectories for Cloud 2 (Fig. 2a and c) show that the air mass spent most of the previous 96 h over the Pacific Ocean and arrived at the sampling site from a northwesterly direction. During the first part of Cloud 2 (from 12 June 21:00 to 13 June 08:00 PDT) the back trajectories became progressively more northerly and the air mass began traveling near large populated urban regions. Towards the end of the cloud event (at ≈09:00 PDT on 13 June) the winds shifted to southwesterly. Based on the back trajectories the air mass for Cloud 2 traveled ≈40-50 km over land before reaching the sampling site. In addition, the air mass spent a significant amount of time close to the ocean surface prior to being lifted up to the sampling site (Fig. 2c).

The back trajectories for Cloud 3 (Fig. 2b and d) also show that the air mass spent the majority of the previous 96 h over the Pacific Ocean before arriving at the site. At the start of Cloud 3 (17 June 21:00 to 22:00 PDT) the air mass arrived from the northwest. Throughout the remainder of the cloud event (17 June 23:00 to 18 June 08:00 PDT) the air mass continued to shift farther north and by the end of the cloud event (18 June 08:00 PDT) the air mass was traveling south along the coastline before arriving at the sampling site. The back trajectories indicate that the air mass traveled ≈10-20 km over land prior to arriving at the sampling site. Similar to Cloud 2, the air spent a significant amount of time close to the ocean surface prior to

being lifted up to the sampling location (Fig. 2d). Since the trajectories during both clouds are close to the coastline for a period of time, it is likely these air masses contained both marine particles and anthropogenic emissions.

3.2. Meteorological conditions and cloud properties

For the purposes of this study, the data were classified as in-cloud and included for analysis if they met the following criteria: (1) the five minute averaged CVI counterflow was within ±~~5σ~~6% of the mean counterflow (i.e. ±5σ, where σ is standard deviation) to ensure only periods of stable CVI flows were included; and (2) the five minute averaged LWC was greater than 0.05 g m^{-3} to remove periods of entrainment, or "patchy" regions of the cloud as much as possible (Cozic et al., 2007).

The measured cloud properties as a function of time are shown in Fig. 3a-c, where Cloud 2 is shown on the left side and Cloud 3 is shown on the right side of the plot. Cloud 2 was characterized by ~~an average~~a median temperature of 13.4 ~~± 0.2~~ °C, a median wind velocity of ~~with light and variable winds (~~ 0.5 ~~± 0.2~~(10th and 90th percentiles of 0.3and 0.8) m s^{-1} and ~~190 ± 90~~ median wind direction of 126° (10th and 90th percentiles of 60 and 297° ~~respectively~~), and ~~an average~~ a median LWC of 0.1~~03 ± 0.07~~ g m^{-3}. During the middle portion of Cloud 2 (13 June 01:00 to 02:00 PDT) the droplet distributions clearly show an interval where the number of droplets above the CVI– D_{50} (black trace overlaid on panel C) increases significantly, which coincides, in time, with a sharp increase in LWC. Cloud 3 was characterized by ~~an average~~a median temperature of 15.2 ~~± 0.1~~ °C, a median wind velocity of 1.4 m s^{-1} (1oth and 90th percentiles of 1.1 and 2.0 m s^{-1}), a median wind direction of 328 °C (10th and 90th percentiles of 322 and 341 °C) and a median LWC of 0.09 g m^{-3}. ~~northerly (330 ± 10°) winds with an average speed of 1.5 ± 0.4 m s^{-1}, and an average LWC of 0.09 ± 0.02 g m^{-3}.~~

The cloud droplet number and volume size distributions, averaged over the entire event, are shown in Fig. 4, and further summarized in Table 1. Cloud 3 had a CDNC of 146 cm^{-3}, a factor of two higher than during Cloud 2 (68 cm^{-3}).

From the calculated CVI– D_{50} and the fits to the droplet size distribution (Fig. 4) the number and volume fraction of droplets sampled by the CVI were determined. The results are summarized

in Table 1. During Cloud 2 the number fraction of droplets larger than the CVI– D_{50} was about 38 % and for Cloud 3 the fraction sampled was about 24 %. Since only the larger droplets were sampled by the CVI during these two cloud events, the results presented herein are only representative of the larger droplet population.

3.3. Size Distributions

Average size distributions of the bulk aerosol particles and rBC particles measured from the total and residual inlets for both cloud 2 and cloud 3 are shown in Fig.5. Data are plotted in two ways; on a log scale, in panels A and B and normalized to the respective maximum, in panels C and D. Table 2 summarizes the results obtained from the size distribution analysis. All size distributions shown in Fig. 5 have been corrected for differences in instrument sensitivity, and all residual distributions have been corrected for the CVI enhancement factor (see Supplementary Material Sect. S1) and droplet transmission through the CVI (see Supplementary Material Sect. S4).

3.3.1. Size distributions measured from the total inlet ($BulkAero_{Tot}$ and rBC_{Tot})

The average size distributions of the bulk aerosol measured with the total inlet (referred to as $BulkAero_{Tot}$ for the remainder of the document) and the average size distributions of the refractory black carbon measured with the total inlet (referred to as rBC_{Tot} for the remainder of the document) are shown in Fig. 5. ~~The $BulkAero_{Tot}$ distributions for both clouds show evidence of at least two overlapping modes.~~ A single mode lognormal distribution function was fit to the $BulkAero_{Tot}$ data yielding mean geometric diameters (D_g) of 108 and 81nm with geometric standard deviations (σ_g) of 1.58 and 1.70 for Cloud 2 and 3 respectively. Integration of the number distribution during Cloud 2 results in a total number concentration (N_{Tot}) for the bulk aerosol of 981 cm^{-3}. Likewise, N_{Tot} during cloud 3 were measured to be 994 cm^{-3}. Previous measurements in the marine boundary layer have classified the environment as "clean" marine if the number of particles is ≤300-500 cm^{-3} and "polluted" marine if the number concentrations are ≥400-1500 cm^{-3} (Andreae, 2009; Bates et al., 2000; Glantz and Noone, 2000; Hawkins et al., 2010; O'Dowd et al., 2001; Pirjola and O'Dowd, 2000; Twohy et al., 2005). Thus the particle

concentrations measured at Mt. Soledad, in addition to the back trajectories, suggest that for both clouds the air masses can be classified as polluted marine aerosols. The size distributions of $BulkAero_{Tot}$ as a function of time are also included in Fig. 3d for comparison.

The rBC_{Tot} size distributions for each cloud are shown in Fig.5. The D_g for rBC_{Tot} (assuming the number distributions are lognormal) during both events lies somewhere in the nucleation mode at <70 nm, which is outside the detection range for the SP2. Integration of the rBC_{Tot} distributions, from 70-220 nm, yields an N_{Tot} of 75 cm^{-3} during Cloud 2 and 62 cm^{-3} in Cloud 3. Assuming a black carbon density of 1.8 cm^{-3} the total mass concentrations of rBC (M_{Tot}) are 73 and 62 ng m^{-3} for Clouds 2 and 3 respectively (Table 2). The rBC_{Tot} mass concentrations observed at Mt. Soledad were higher than concentrations measured in clean marine air (Cooke et al., 1997; Shank et al., 2012), but considerably lower than concentrations measured in most urban environments (see Table 1 in Metcalf et al., 2012).

3.3.2. Size distributions measured from the residual inlet ($BulkAero_{Res}$ and rBC_{Res})

Average size distributions of the bulk aerosol measured from the residual inlet (referred to as $BulkAero_{Res}$ for the remainder of the document) are also shown in Fig. 5. The size distributions of the $BulkAero_{Res}$ indicate that it was mostly the larger particles of the $BulkAero_{Tot}$ distributions that were incorporated into the sampled cloud droplets. The size distributions of $BulkAero_{Res}$ as a function of time for both cloud events are included in Fig. 3e for comparison.

The size distributions for $BulkAero_{Res}$ shown in Fig. 5 have a local minimum at 110 nm for Cloud 2 and 90 nm for Cloud 3. The particles observed at sizes less than the local minima may be due droplet ~~"splash"~~shattering, or due to a leak in the CVI (Pekour and Cziczo, 2011; Schwarzenboeck, 2000; Vidaurre et al., 2011), or possibly due to entrainment or precipitation processes in the clouds (Targino et al., 2007).

Figure 5 also shows the size distributions of the rBC residuals measured with the CVI. Figure 5 shows that rBC cores smaller than 100 nm are incorporated into cloud droplets. In addition, ~~Fig.5 shows that most of the rBC_{Res} have effective sizes of less than 100 nm and rBC_{Res}~~ they are overall larger than the rBC_{Tot}. Fitting the rBC_{Res} size distributions (assuming these distributions are lognormal) results in mean geometric diameters of 87 and 81 nm for Cloud 2 and 3

respectively.

3.4. Size resolved activated fraction

The size resolved activated fraction [AF(Dp)] for rBC and the bulk aerosol were calculated by taking the ratio of the number distributions measured with the residual inlet to the number distributions measured with the total inlet. Prior to calculating AF(Dp), a spline interpolation algorithm was applied to the rBC and bulk aerosol size distributions. After a spline interpolation was applied to the data, the following equation was used to calculate the size resolved activated fraction:

$$AF(D_p) = \frac{N_{Res}(D_p) \times CF(D_p)}{N_{Tot}(D_p) \times EF \times DT} \quad (1)$$

where N_{Res}(Dp) is the number of residual particles as a function of size, CF(D_p) is the size-resolved instrument sensitivity correction factor, N_{Tot}(Dp) is the number of particles measured with the total inlet as a function of size, EF is the CVI enhancement factor (~~Appendix A~~Supplementary Material Sect. S1) and DT is the droplet transmission factor through the CVI. Calculations of the droplet transmission factor are given in ~~Appendix C~~the Supplementary Material Sect. S4 and plotted i~~f~~n Fig. ~~A1~~S3. CF(D_p), which correct for variances in instrument detection efficiencies, were determined from a 12 h period of cloud free air on 5 June 2012 for the bulk aerosol and from side by side ambient sampling of room air during the post-campaign for rBC. Additional information on the measurement of CF(D_p) for rBC is given in the Supplementary Material (Sect. S2).

The median AF(Dp) for the bulk aerosol and rBC are presented in Fig. 6, where the error bars represent ~~one standard deviation (1σ)~~the 10th and 90th percentiles ~~of the AF~~ for each 10 nm bin. ~~The AF as a function of size for the bulk aerosol is similar to previous measurements in similar clouds (Hallberg et al., 1994).~~ Uncoated rBC particles with sizes < 100 nm are not expected to be incorporated into cloud droplets by nucleation for typical supersaturations reached in stratocumulus clouds. Figure 6 a and b show that the AF of rBC cores is significant, even for ~~a~~ core diameter~~s of~~ ≤100 nm. These results can be explained by the presence of large coatings surrounding the core (See Sect. 3.6 below). Since the rBC size distributions were normalized to differences in instrument sensitivity, the decreased rBC AF at

smaller diameters is not a result of the different detection efficiencies of the SP2 instruments. Figure a and b also show that during both clouds the AF for rBC cores is larger than the AF for the bulk aerosol at diameters less < ≈ 150 nm. Again, this can be explained by the presence of thick coatings on the rBC cores. ~~These results can be explained by the presence of large coatings surrounding the core (see section 3.5).~~ Since the fraction of cloud droplets sampled by the CVI was < 100 %, the calculated AF should be considered as lower limits to the total fraction activated during the two cloud events.

3.5. Mechanism of incorporating rBC into cloud droplets

Two possible mechanisms exist for incorporating rBC containing particles into cloud droplets: nucleation scavenging and coagulation between the rBC containing particles and cloud droplets. Results and calculations suggest that the dominant mechanism for incorporating rBC particles into the cloud droplets studied was nucleation scavenging. First, the fraction of rBC containing particles activated into cloud droplets increases as the size of the rBC cores increases (see Fig. 6a and b). If coagulation dominated we would expect to see an opposite trend. Second, calculated coagulation rates, together with estimated lifetimes of the cloud droplets cannot explain the fraction of rBC containing particles activated into the cloud droplets - the calculated coagulation rates are too small (see Supplementary Material Sect. S3).

~~3.5.~~3.6. Lower limits to ~~C~~coating thickness of rBC residuals

Lower limits to the ~~C~~coating thicknesses on the rBC cores were determined using a core and shell Mie model. ~~and~~ The median values ~~are~~ from this analysis are shown in Fig.6c and d, where the error bars represent ~~1σ and the symbols represent the averages.~~the 10th and 90th percentiles and the symbols represent the medians for each size bin. When calculating lower limits to the coating thicknesses, the particles were idealized as a pure BC core uniformly coated with a non-absorbing material, although the actual particle morphology may be more complicated (Sedlacek et al., 2012). ~~As mentioned in Sect. 2.5, only 50% of the rBC containing particles detected with the SP2$_{Res}$ were successfully fit with the LEO fitting procedure. Hence, coating information reported below is only from a subset of the rBC residual particles measured.~~ The results shown in Fig. 6c and g give a qualitative explanation for why we see activation of rBC cores with sizes < 100 nm: these rBC cores have relatively thick coatings, which can lower the critical

supersaturation required for activation. For example, 95 nm rBC cores incorporated into the cloud droplets had a median coating thickness of 65 nm.

~~Both cloud events show a similar trend, namely that the coating thicknesses are larger at smaller rBC core diameters than larger rBC core diameters, which has also been observed elsewhere (Metcalf et al., 2012). At small core diameters (70-100 nm) the coating thicknesses range from roughly 45-115 nm, while at larger core diameters (200-215 nm) the coatings range from roughly 0-60 nm. Coating thicknesses measured in this study fall between values measured in previous studies. For example, coating thicknesses ranging from 20 ±10 nm, in fresh urban plumes (Schwarz et al., 2008a), up to 188 ± 31 nm on more aged rBC particles (Metcalf et al., 2012) have been reported.~~ Figure 6c and d shows that as the rBC core diameter increased from 75 to approximately 100 nm the lower limit to the coating thickness also increased. This is likely because as the rBC core diameter increased from 75 to 100 nm, the fraction of particles above the optical detection limit increased. Recall, that for rBC containing particles with diameters < ≈100 nm a relatively large fraction of the coated particles are below the optical detection limits and hence are assigned a coating thickness of zero (see Sect. 2.5). After the median coating thickness reached a maximum at an rBC core diameter of approximately 100 nm, the lower limit to the coating thickness decreased with an increase in rBC core diameter. This may suggest that the larger rBC cores had thinner coatings then the smaller rBC cores that were incorporated into the cloud droplets. Part of the decrease in the lower limit to the coating thickness with an increase in rBC core diameter could be due to saturation of the optical detector. As mentioned in Sect. 2.5, the optical detector became saturated when the rBC cores were relatively large and contain a modest coating. For example, the scattering from a 220 nm rBC core with a coating thickness of 40 nm will saturate the detector.

In Fig. 6c and h we plotted the overall diameter of the rBC containing particles. In other words, we plotted the sum of the rBC core diameter plus 2 x the coating thickness. If we disregard the point at 75 nm (which is likely strongly influenced by the fact that a large fraction of the rBC containing particles, with this core size, are below the optical detection limit) we conclude that in order for the rBC containing particles to be incorporated into the cloud droplets the overall median diameter of rBC containing particles must be at least 165 nm in diameter. Figure 6c and h suggest that the overall diameter of the rBC containing particles is important for activation. This finding is consistent with previous work that has shown that particle diameter is

important for activation of non-rBC containing particles (e.g. see Wang et al., 2008).

To further investigate the factors that control activation of the rBC containing particles we plotted the coating volume (Fig. 6d and h) and coating volume fraction (Fig. 6e and j) as a function of rBC core diameter. For discussion purposes we focus on the coating volume fraction as a function of size and rBC core diameters ≥ 85 nm. As discussed above, coating volume fraction at 75 nm rBC core diameter, is likely strongly influenced by the fact that a large fraction of rBC containing particles, with this core size, are below the optical detection limit. Figure 6e and j show that for rBC core diameters from 85 to 95 nm, the median coating volume fraction is at least 0.9. This finding also gives a qualitative explanation for why we see relatively large activated fractions of small rBC cores in the cloud residuals.

As the rBC core diameter increased past approximately 100 nm, the lower limit to the coating volume fraction decreased. This could be because larger rBC cores need less coating material in order to be incorporated into cloud droplets. Part of the decrease in coating volume fraction at rBC core diameters above 100nm could also be due to the saturation limit of the optical scattering detectors, as discussed above.

3.7. In-cloud aqueous phase chemistry

In the discussion above, we assume the coatings on the rBC cores were present before incorporation into the cloud droplets. However, some of the coating material may have formed after the rBC cores were incorporated into the cloud by aqueous phase chemistry. As mentioned in the Supplementary Material, the upper limit to residence times of air parcels in the clouds sampled at Soledad were likely 1 h. Whether significant aqueous phase chemistry can occur on this time scale depends on the level of SO_2 and oxidants. When SO_2 is absorbed by a cloud droplet, it partitions in different forms as a function of pH: at lower pH values, the primary aqueous phase oxidant of dissolved SO_2, or S(IV) is H_2O_2; for higher pH values, ozone and catalyzed aerobic oxidation are important oxidation pathways. Depending on the pH and available oxidants, conversion of the dissolved S(IV) to S(VI) can be fast or slow. The absorption of large amounts of HNO_3 or N_2O_5 can reduce the pH significantly, which will require the presence of H_2O_2 in order to significantly convert S(IV) to S(VI). Since the clouds at Soledad were mostly overnight, the primary oxidant (H_2O_2) was likely lower (and probably near zero). Also, analysis of the cloud water indicated that nitrate was high, and thus the pH was

probably low. Based on these factors, we suspect that aqueous phase production of sulfate was not large. However, a quantitative estimate of the sulfate produced is not possible since the measurements of SO_2 and H_2O_2 were not performed at this site. Based on the discussion above, we assumed that a large fraction of the coatings were present before rBC particles were incorporated into the cloud droplets. However, the production of coating material from in-cloud aqueous phase chemistry cannot be ruled out.

~~**3.6. Size distributions of rBC_{Res} (Core + Coating)**~~

~~For every rBC particle measured, with the residual inlet, a core diameter (determined from the incandescence signal) and a coating thickness (determined from the Mie scattering calculations discussed in section 2.4) were combined to calculate the overall rBC particle diameter (Core + Coating). These data are plotted in Fig. 5 (purple lines), where the distributions are shown to be shifted to larger sizes when compared with the distributions plotted as a function of the core diameter (rBC_{Res} (Core)) alone. Furthermore, incorporating the coating into the rBC size distribution results in a greater similarity between the size distributions of the bulk aerosol and rBC.~~

~~3.7.~~3.8. Comparison of rBC_{Res} as a function of size with predictions based on κ-Köhler theory

Sections 3.4 and 3.~~5~~ 6 provide a qualitative explanation for ~~why~~ how small rBC cores ~~smaller than 100 nm~~ are incorporated into cloud droplets – the rBC cores have thick coatings which leads to overall particles diameters ~~>~~greater than approximately 165~~00~~ nm. In the following we expand on this qualitative explanation by carrying out a quantitative analysis that shows that the presence of small rBC cores ~~smaller than 100 nm~~ in the cloud residuals is consistent with kappa-Köhler theory. This quantitative analysis consists of the following steps: (1) an estimation of the bulk aerosol composition; (2) an estimation of the critical diameter for activation of the cloud droplets sampled; (3) an estimation of the critical supersaturation required to form the droplets sampled, and (4) a prediction of the critical diameter for activation of rBC cores. Steps 1-3 are required to carry out the predictions in step 4.

~~3.7.1.~~3.8.1. Bulk aerosol composition

A HR-ToF-AMS was used to measure the bulk aerosol composition in residual particles downstream of the CVI. Five species (organic, nitrate, sulfate, ammonium and chloride) were quantitatively differentiated. Then, based on a simplified ion-pairing scheme similar to (Gysel and Crosier, 2007) (see ~~Appendix B~~Supplementary Material Sect. S5), the mass fractions of ammonium nitrate, ammonium sulfate, ammonium bisulfate, sulfuric acid, and ammonium chloride were calculated. The results of these calculations are shown in Fig.~~8~~7. In order to determine the bulk aerosol hygroscopicity (see Eq. 3) mass fractions, of these individual components, were first converted to volume fractions using and organic density of 1.4 g cm^{-3} (Moore et al., 2012) and densities report in Lide, 2001 for the inorganic salts.

~~3.7.2.~~3.8.2. The critical diameter for activation of the bulk aerosol in the cloud droplets sampled

The critical diameter for activation (D_{crit}) of the bulk aerosol is often calculated by integrating the droplet number distribution from the largest to smallest diameters until the number concentration equals the CDNC sampled (see for example Hersey et al., 2013). Using this method, D_{crit} was found to be 241 nm and 239 nm for Cloud 2 and Cloud 3, respectively. Note these D_{crit} values apply only to the cloud droplets sampled (i.e. cloud droplets greater than ≈ 11 μm). Different D_{crit} values would be expected if the entire cloud droplet population were sampled.

~~3.7.3.~~3.8.3. Critical supersaturation for the cloud droplets sampled during the two cloud events.

To estimate the critical supersaturation (S_C) for the formation of the cloud droplets sampled during the two cloud events (i.e. cloud droplets greater than ≈ 11 μm) the single parameter kappa-Köhler model (Petters and Kreidenweis, 2007) was used. This model describes the relationship between the water vapor saturation ratio (S) over an aqueous solution droplet, and can be calculated using the following equation:

$$S = \frac{D^3 - D_p^3}{D^3 - D_p^3(1-\kappa_{Bulk})} exp\left(\frac{4\sigma M_w}{\rho_w RTD}\right) \quad (2)$$

where D is the droplet diameter; D_p is the dry particle diameter; σ is the droplet surface tension,

and is assumed to be that of water, 0.072 J m^{-2}; M_W is the molecular ~~weight~~ mass of water; ρ_W is the density of water; R is the universal gas constant; T is the temperature; and κ_{Bulk} is a compositionally specific parameter that describes the bulk aerosol's hygroscopicity. Equation (2) was used to find the S_C needed for a particle of dry diameter D_p to activate (Petters and Kreidenweis, 2007).

The overall hygroscopicity of a particular aerosol follows a simple mixing rule and can be calculated from:

$$\kappa_{Bulk} = \sum_i \varepsilon_i \kappa_i \quad (3)$$

where ε_i is the volume fraction and κ_i is the hygroscopicity parameter for each component i discussed in Section 3.~~8~~7.1. The individual component κ values used in equation 2 were; 0.1 for organic (Lance et al., 2013; Moore et al., 2012; Rose et al., 2010); 0.67 for ammonium nitrate (Petters and Kreidenweis, 2007); 0.61 for ammonium sulfate and ammonium bisulfate (Petters and Kreidenweis, 2007; Wu et al., 2013); and 0.71 for sulfuric acid, which is the average of the range reported in Shantz et al., 2008. The value for ammonium chloride κ was calculated according to Eq. (A28) in (Rose et al., 2008) using a Van't Hoff factor of 2.

Using the above κ_i values and the ε_i values discussed in Section 3.~~8~~7.1 in Eq. (3), κ_{Bulk} values of 0.50 and 0.41 were calculated for Cloud 2 and Cloud 3 respectively. The values determined during this study are consistent with the values suggested by Andreae and Rosenfeld, 2008 for Cloud 2 and lower than the values suggested for Cloud 3.

Shown in Fig.~~9a~~ 8a are plots of S_C as a function of dry diameter for Cloud 2 (solid line) and Cloud 3 (dashed line) calculated using Eqs. (2) and (3). Combining D_{crit} (see Section 3.~~8~~7.2) with the results plotted in Fig. ~~9~~8, S_C for the cloud droplets sampled can be determined. The points at which D_{crit} intersect with the calculated S_C traces shown in Fig ~~9~~8, result in estimations of S_C values of 0.05% for both clouds. Note these critical supersaturations apply only to the cloud droplets sampled by the CVI. Different S_C values would be expected if the entire droplet population had been sampled. Theory predicts that the largest droplets in the

distribution should have been the first to form, thus formed on particles activated at the lowest supersaturations. During this study a CCN instrument was also connected to the residual inlet and sampled residual particles during the cloud events. Data from this instrument were used to derive an upper limit to the cloud supersaturation applicable to the cloud droplets sampled by the CVI (manuscript in preparation), and was found to be approximately 0.1%. This upper limit to the cloud supersaturation is consistent with the S_C values reported here using the estimation technique discussed above.

In this determination of S_C several assumptions were made, which are addressed separately below: (1) the predominant mechanism for incorporation of particles into droplets was nucleation scavenging, and influences by impaction were negligible ~~(Noone et al., 1992)~~ (see Sect. 3.5); (2) the contribution from sea salt aerosols could be neglected. Based on sea salt mass concentrations measured by the HR-Tof-AMS behind the CVI and calibrated against collocated ion chromatography measurements following a procedure similar to that introduced by Ovadnevaite et al., 2012, we estimated an upper limit of approximately 15% for the sea salt mass fraction of the cloud residuals (these results will be discussed in detail in a future publication). A sensitivity study (not shown here) indicated a < 8% decrease in the estimated S_C when a sea salt fraction of 15% was include; (3) we assumed that the particles were internally mixed and the composition did not depend on size. Since, during this study, the size dependent AMS data were at or below the detection limit we could not determine if the composition was size dependent. Additionally, no measurements of bulk aerosol mixing state were carried out; and (4) we assumed that the entire fraction of organics was water soluble and represented by a κ of 0.1. To determine if S_C was sensitive to this value, κ for organics was varied from 0-0.2, which is roughly consistent with the range of κ values reported in the literature for organics (Chang et al., 2010; Lathem et al., 2013; Mei et al., 2013). Over this range of κ values, S_C varied by < 4%.

~~3.7.4.~~3.8.4. Predictions of the critical diameter for activation of rBC cores

In Fig. ~~9b~~ 8b the critical diameter for activation of rBC cores for the cloud droplets sampled is

calculated using kappa-Khöler theory and assuming coating thicknesses ranging from 0-200nm, which covers the range of coating thicknesses measured. In these calculations the composition of the coating was assumed to be the same as determined by the AMS (see Section 3.~~7~~8.1), and the rBC cores were assumed to be insoluble with a κ=0 (Rose et al., 2010). As expected, in Fig.~~8~~9b, S_C decreases as the coating thickness increases at a constant rBC core diameter. Figure ~~8~~9b also ~~shows~~suggests, that if the S_C is ~~>~~ ≈0.05%, and the diameter of the rBC core is 95 nm, the coating thickness must be between 50 and 75 nm. Our lower limits to the coating thicknesses for an rBC core diameter of 95 nm shown in Fig. 6b and g are consistent with these predictions. ~~for both clouds, the critical diameter for activation of the rBC cores is < 50 nm for all cores with coatings >= 100nm. This quantitative prediction is consistent with rBC cores of 100 nm and less being activated into the sampled cloud droplets.~~

In Fig. 8c we plotted S_C as a function of the rBC coating volume fraction assuming rBC core diameters of 75 nm, 100 nm and 200 nm. This figure illustrates that in order to activate 75 and 100 nm rBC cores at a S_C of 0.05% the rBC coating volume fraction must be greater than 0.9. Figure 9c also shows that for an rBC core diameter of 200 nm, the coating volume fraction needs to be approximately 0.6. For 100 nm rBC cores the measurements are in good agreement with the predictions (compare Fig. 9c with Fig. 6e and j). For 75 nm cores and 200 nm cores the measurements are lower than the predictions. However, the measurements are not inconsistent with the calculations since the measurements are lower limits.

4. Summary and conclusions

Cloud residuals were measured during two cloud events at the top of Mt. Soledad in La Jolla, CA. Back trajectories showed that air masses for both cloud events spent at least 96 h over the Pacific Ocean and traveled near, or over populated regions before arriving on site. Based on measured bulk aerosol concentrations the two air masses sampled were classified as polluted marine air, a classification consistent with the back trajectories and measured concentrations of black carbon.

~~The s~~Size distributions of the bulk aerosol residuals were shifted to larger sizes for both cloud events compared to size distributions measured with the total inlet. The size distributions of rBC cloud residuals were also shifted towards larger diameters when compared to the size distributions of rBC measured with the total inlet. ~~The measurements of the cloud residuals clearly show that rBC cores less than 100 nm can be incorporated~~

~~into cloud droplets and therefore contribute to the CCN population. The activated fraction of 70-80 nm rBC cores was 0.01 and 0.045 for Clouds 2 and Cloud 3 respectively.~~ The activated fractions of rBC determined from the measurements ranged from 0.01 to 0.1 for rBC core diameters ranging from 70 to 220nm. This type of data will be useful for constraining models used to predict rBC concentrations in the atmosphere. -Since the fraction of cloud droplets sampled by the CVI was less than 100 %, the measured activated fractions of rBC are lower limits to the total fraction of rBC activated during the two cloud events.

To investigate the factors that control the incorporation of rBC into cloud droplets, we determined lower limits to the coating thickness, the total diameter (rBC core + coating), the coating volume and the coating volume fraction of the rBC cores incorporated into cloud droplets. Uncoated rBC particles with diameters < 100 nm are not expected to be incorporated into the cloud droplets sampled at Mt. Soledad due to the high supersaturations required for nucleation of uncoated 100 nm rBC particles and the low critical supersaturations often observed for stratocumulus clouds. The coating thicknesses give a qualitative explanation for why we see relatively large activated fraction of rBC cores with sizes < 100 nm – the rBC cores with sizes < 100 nm have relatively thick coatings, which increases the overall size of the rBC containing particles and provides soluble material to the particle which can lower the critical supersaturation required for activation. The measurements of the coating volume fraction show the median coating volume fraction was at least 0.9 for rBC core diameters ranging from 85-95 nm, a result consistent with kappa-Köhler theory. The measurements of the total diameter (rBC core + coating) suggest that the total diameter must be at least 165 nm in diameter in order for rBC cores with diameters ≥ 85 nm to be incorporated into cloud droplets. The results also suggest that the total particle diameter (core + coating thickness) is important for determining if rBC particles are incorporated into the cloud droplets. This finding is consistent with previous work that has shown that particle diameter is important activation of non-rBC containing particles (Wang et al., 2008). ~~The coating analysis of the SP2 data shows that the rBC cores that were activated into cloud droplets had thick coatings, with average coating thicknesses of ≈ 75 nm at core diameters between 70 - 80 nm and ≈ 29 nm at core diameters between 210 - 220 nm. The presence of rBC cores less than 100 nm in~~

~~cloud residuals is consistent with κ-Khöler theory and measured rBC coating thicknesses.~~

Acknowledgements

The authors would like to thank D. Toom-Sauntry, S. Sharma, and A. Sheppard, from Environment Canada, as well as A. Lee, and R. Zhou, from the University of Toronto, for their contributions during the campaign and the three anonymous referees for very helpful feedback on the manuscript. The authors are also grateful for funding provided by Environment Canada through the Clean Air Regulatory Agenda, NSERC, NSF (grant AGS1013423), and the FORMAS MACCII project.

Figures

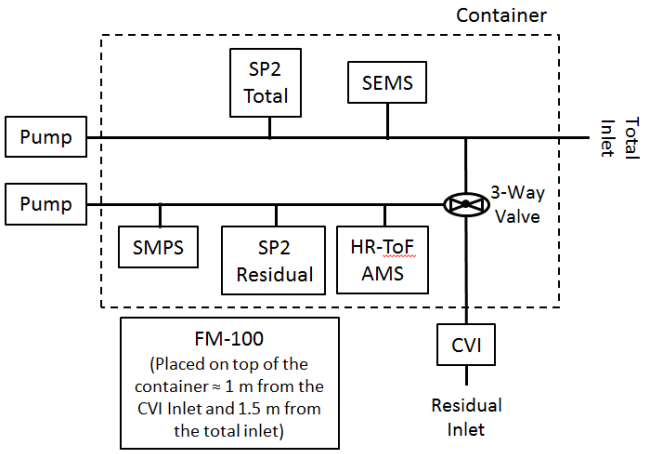

Fig. 1. Schematic showing the configuration of the inlets and instrumentation housed in the shipping container

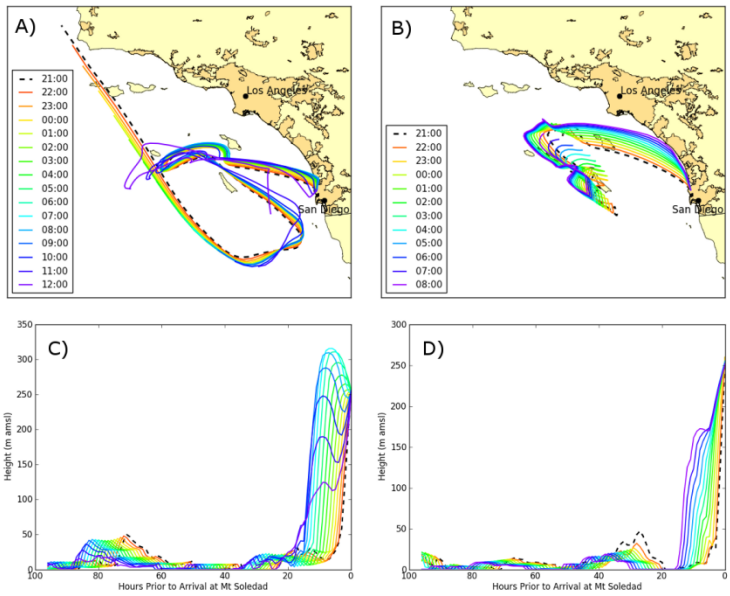

Fig. 2. In-cloud HYSPLIT 96hr back trajectories ending at hourly intervals for Cloud 2 (12 June 21:00 13 June 12:00 PDT) in panels A and C, and Cloud 3 (17 June 21:00 to 18 June 08:00 PDT) in panels B and D. All back trajectories started at 10 m a.g.l. Darker yellow regions on land in panels A and B indicate densely developed urban areas containing 50,000 or more people (United States Census Bureau). Panels C and D show the vertical profiles over the same hourly intervals shown in panels A and B.

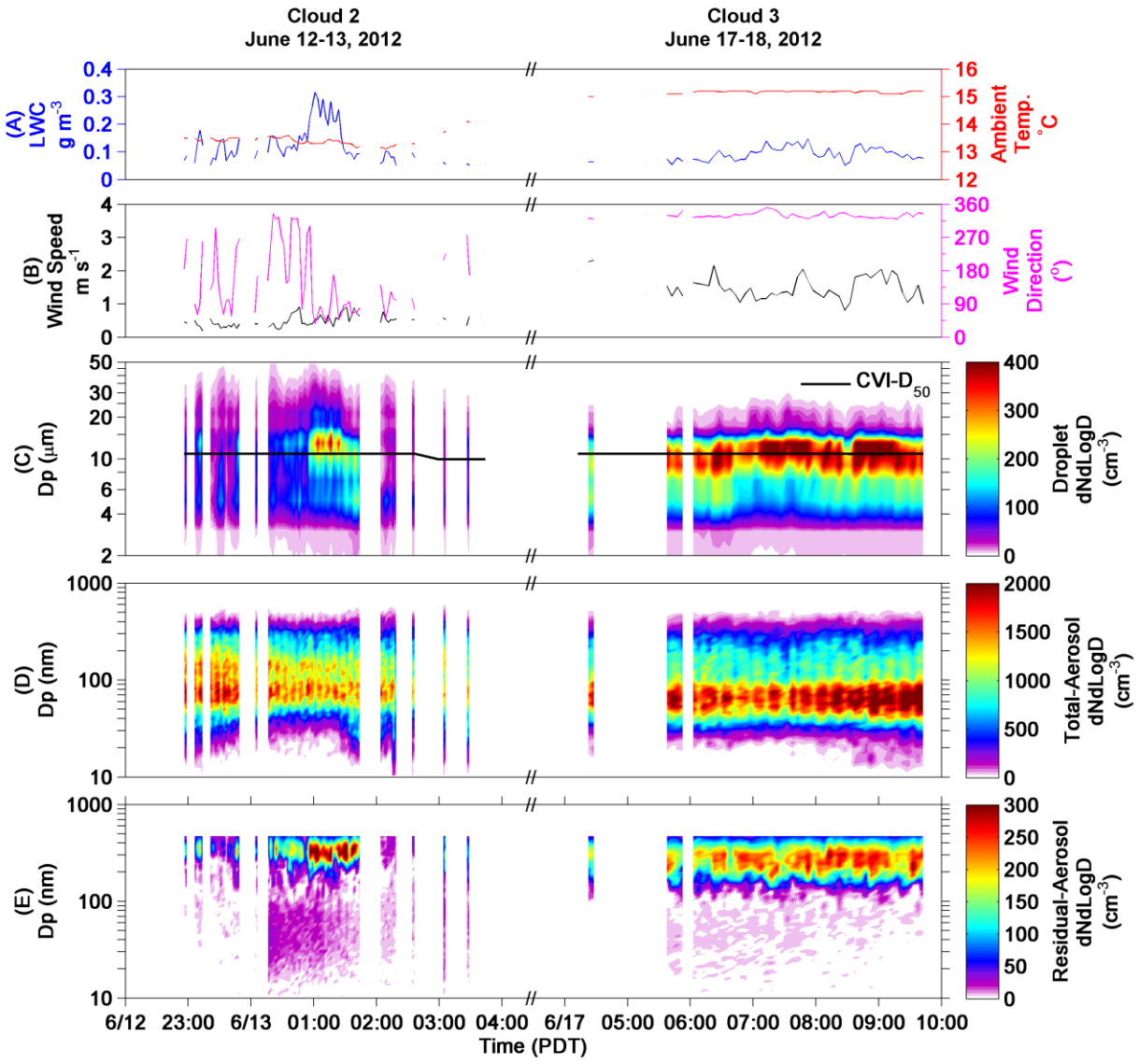

Fig. 3. Time series data for both Cloud 2 (left side) and Cloud 3 (right side) showing; liquid water content (LWC, blue trace) and ambient temperature (red trace) in panel A; wind speed and direction in panel B; cloud droplet number size distributions with the CVI-D_{50} (black trace) overlaid in panel C; the number size distribution for the total aerosol in panel D, and the residual aerosol in panel E. All data shown are five minute averages and meet the criteria discussed in the text.

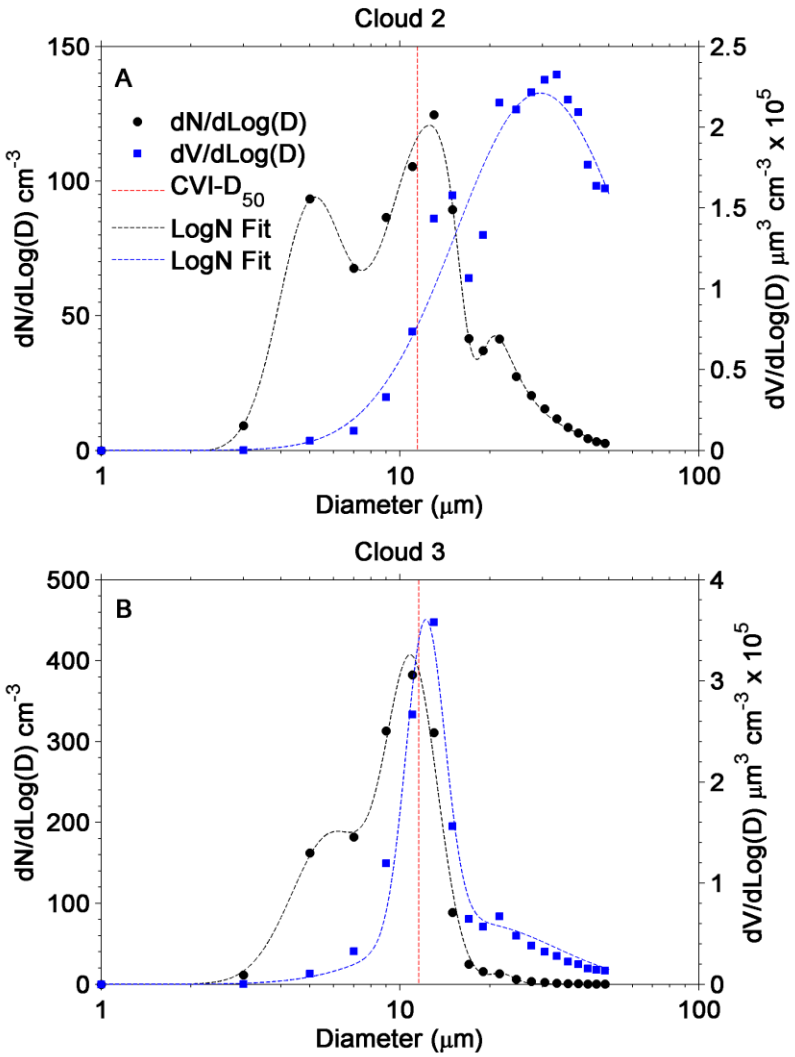

Fig. 4. Average cloud droplet number size distributions for Cloud 2 (panel A) and Cloud 3 (panel B) measured by the FM-100 (black circles) and fit to a lognormal distribution function (black dashed lines). The average cloud droplet volume distributions (blue squares) and lognormal fits (blue dashed lines) are also shown for each cloud event. The CVI-D_{50} is indicated on each panel by a red dashed line.

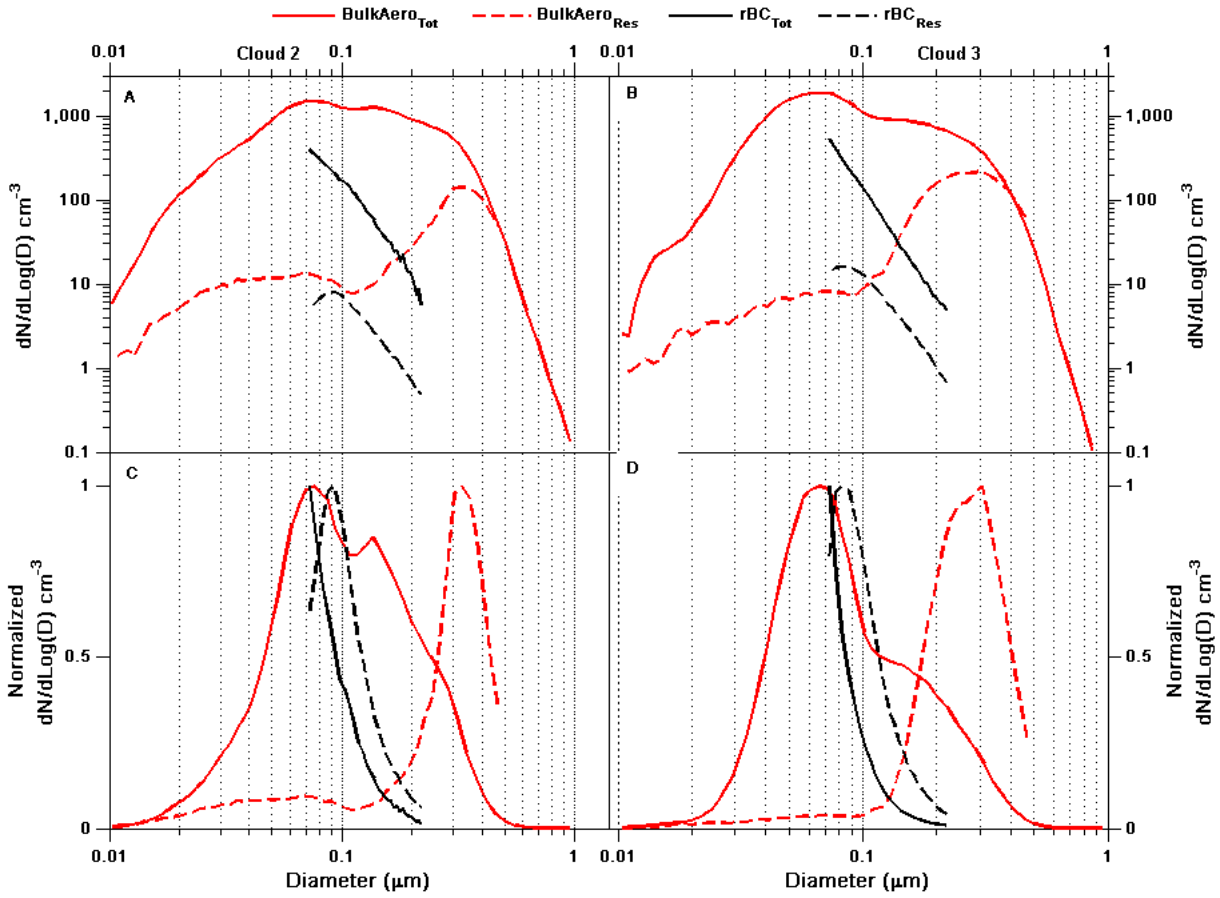

Fig. 5. Summary of the averaged number size distributions for Cloud 2 (panels A and C) and Cloud 3 (panels B and D) for the total aerosol (red solid lines); residual aerosol (red dashed lines); total rBC as a function of core diameter (black solid lines); residual rBC as a function of core diameter (black dashed lines). Both the aerosol and rBC for each cloud event are shown in two ways, a log scale (panels A and B) to highlight the relative differences between the aerosol and rBC as well as normalized to the respective maximum value (panels C and D) to highlight the shift in size distributions. All residual distributions have been corrected for instrument sensitivity (see Fig. 2), CVI enhancement (see A Supplementary Material Sect. S1~~Appendix A~~), and droplet losses (see Supplementary Material Sect. S4~~Appendix C~~).

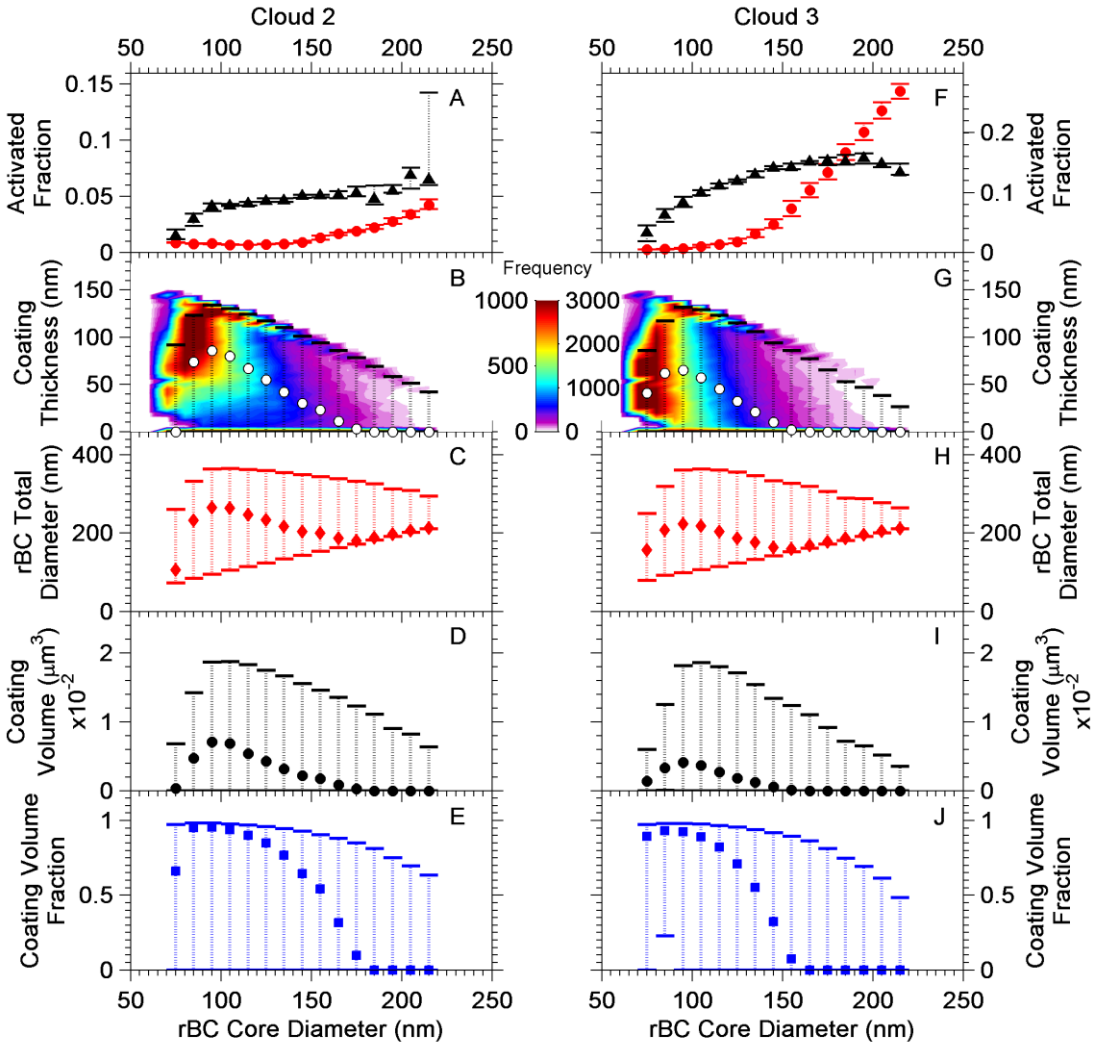

Fig. 6. Shown in panels A and E are the median size dependent activated fraction (AF) for the aerosol (red circles), and rBC (black triangles) for Clouds 2 and 3, respectively, where the error bars represent the 10th and 90th percentiles. The bottom axes represent particle diameter for the aerosol and core diameter for rBC. Panels B and G show a 2D histogram of coating thickness with the median values (white circles) overlaid on top, where the error bars are the 10th and 90th percentiles. Panels C and H show rBC total diameter (i.e. the core + the coating), panels D and I the coating volume, and panels E and J the coating volume fraction, all as a function of rBC core diameter.

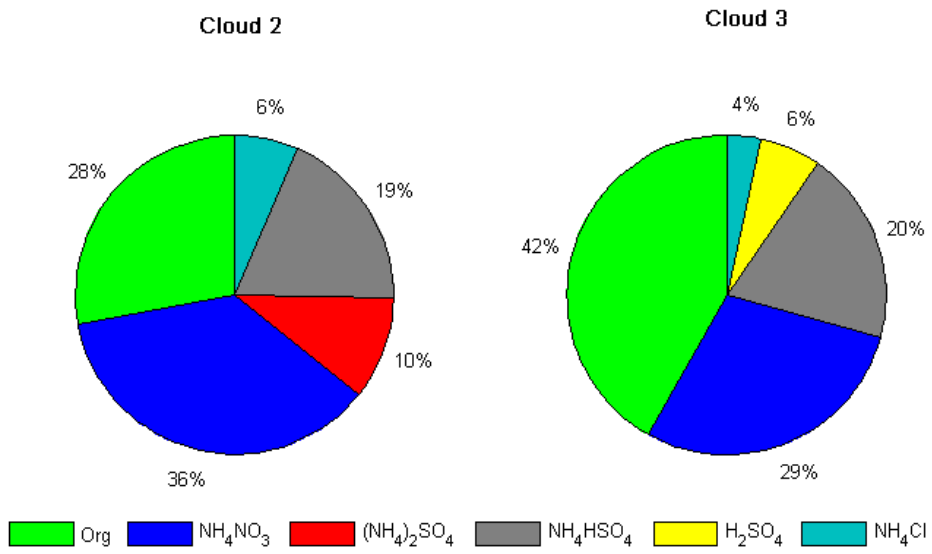

Fig. 7. Sub-micrometer non-refractory average aerosol mass fractions for Clouds 2 and 3 based on an ion-pairing scheme (see text and Supplementary Material Sect. S5~~Appendix B~~) and measured from a high resolution time-of-flight aerosol mass spectrometer.

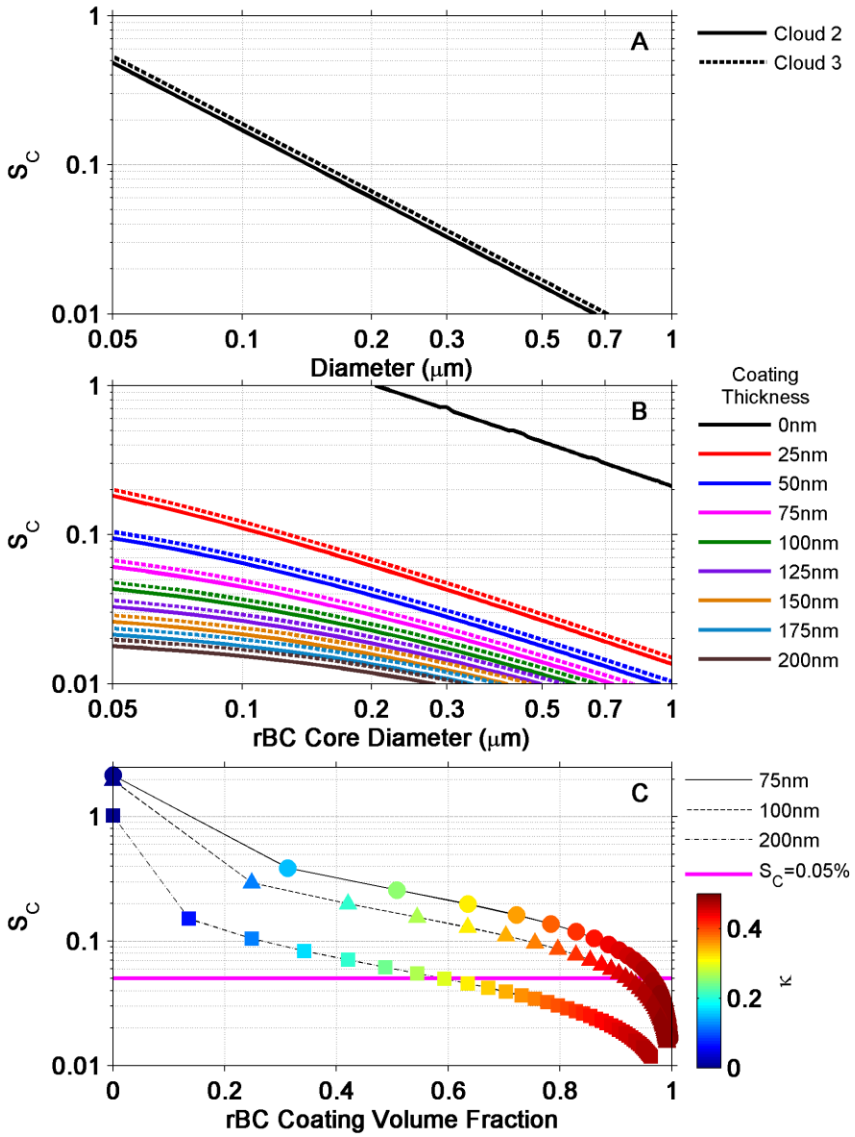

Fig. 8. Panel A shows the critical supersaturation (S_C, black lines) as a function of particle dry diameter based on measured AMS bulk compositions and an ion-pairing scheme. Panel B shows S_C as a function of rBC core diameters with coatings ranging from 0-200 nm. In panel B, the coatings are assumed to have the same composition as the bulk residual aerosol (Fig. 8). The solid lines are for Cloud 2 and the dashed lines are for Cloud 3. Panel C shows S_C as a function of rBC coating volume fraction at three different rBC core diameters (75, 100, and 200nm), where each data point is colored by its corresponding kappa. Also shown on panel C is the estimated S_C (pink line) determined for both clouds in this study.

Tables

Table 1: Summary of cloud microphysical properties showing the average CVI cut-size (CVI-D_{50}) where the uncertainty stems from the calculated cut-size (see text for details); average liquid water content (LWC) and 1 standard deviation; and the cloud droplet number ($CDNC_{Tot}$) and volume (Vol_{Tot})

concentration for droplets with diameters between 2-50 µm. Also shown is the number ($\frac{CDNC_{Samp}}{CDNC_{Tot}}$) and volume ($\frac{Vol_{Samp}}{Vol_{Tot}}$) fractions of droplets sampled, where $CDNC_{Samp}$ and Vol_{Samp} are the number and volume concentrations, respectively, for the fraction of droplets sampled.

Cloud #	Date Sampled	CVI-D_{50} (µm)	LWC (g m^{-3})	$CDNC_{Tot}$ (cm^{-3})	$\frac{CDNC_{Samp}}{CDNC_{Tot}}$	Vol_{Tot} (μm^3 m^{-3})	$\frac{Vol_{Samp}}{Vol_{Tot}}$
2	June 12-13, 2012 20:43-11:35 PDT	11.5 ± 0.72	0.13 ± 0.07	67.67	0.38 ± 0.03	1.24E5	0.91 ± 0.02
3	June 17-18, 2012 20:36-07:52 PDT	11.6 ± 0.72	0.09 ± 0.02	145.8	0.24 ± 0.1	8.88E4	0.68 ± 0.10

Table 2: Averaged number (N) and mass (M) concentrations, modal parameters D_g and σ_g for aerosol and rBC particles during the two cloud events measured at Mt. Soledad. The subscripts Tot and Res represent measurements made from the total and residual inlets respectively.

	Cloud 2		Cloud 3	
	Aerosol	rBC	Aerosol	rBC
N_{Tot} (cm^{-3})	980.8	75.24	994.0	62.13
M_{Tot} (ng m^{-3})	-	73.41	-	61.83
$D_{g,Tot}$ (nm)	107.7	<0.07	80.54	<0.07
$\sigma_{g,Tot}$	1.577	-	1.703	-
N_{Res} (cm^{-3})	43.46	2.000	83.15	3.86
M_{Res} (ng m^{-3})	-	2.741	-	4.735
$D_{g,Res}$ (nm)	331.9	87.30	269.2	80.72
$\sigma_{g,Res}$	1.187	1.259	1.281	1.268

References

Allan, J. D., Delia, A. E., Coe, H., Bower, K. N., Alfarra, M. R., Jimenez, J. L., Middlebrook, A. M., Drewnick, F., Onasch, T. B., Canagaratna, M. R., Jayne, J. T. and Worsnop, D. R.: A generalised method for the extraction of chemically resolved mass spectra from Aerodyne aerosol mass spectrometer data, J. Aerosol Sci., 35(7), 909–922, doi:10.1016/j.jaerosci.2004.02.007, 2004.

Anderson, T. L., Charlson, R. J. and Covert, D. S.: Calibration of a Counterflow Virtual Impactor at Aerodynamic Diameters from 1 to 15 μm, Aerosol Sci. Technol., 19(3), 317–329, 1993.

Andreae, M.: Correlation between cloud condensation nuclei concentration and aerosol optical thickness in remote and polluted regions, Atmos. Chem. Phys., 9(2), 543–556, 2009.

Andreae, M. O. and Rosenfeld, D.: Aerosol cloud precipitation interactions. Part 1. The nature and sources of cloud-active aerosols, Earth-Science Rev., 89(1-2), 13–41, doi:10.1016/j.earscirev.2008.03.001, 2008.

Bates, T. S., Coffman D. J., Covert, D. S. and Quinn, P. K.: Regional marine boundary layer aerosol size distributions in the Indian, Atlantic, and Pacific Oceans: A comparison of INDOEX measurements with ACE-1, ACE-2, and Aerosols99, J. Geophys. Res., 107(D19), 8026, doi:10.1029/2001JD001174, 2002.

Bates, T. S., Quinn, P. K., Covert, D. S., Coffman, D. J., Johnson, J. E. and Wiedensohler, A.: Aerosol physical properties and processes in the lower marine boundary layer: a comparison of shipboard sub-micron data from ACE-1 and ACE-2, Tellus B, 52B, 258–272, 2000.

Baumgardner, D., Popovicheva, O., Allan, J., Bernardoni, V., Cao, J., Cavalli, F., Cozic, J., Diapouli, E., Eleftheriadis, K., Genberg, P. J., Gonzalez, C., Gysel, M., John, a., Kirchstetter, T. W., Kuhlbusch, T. a. J., Laborde, M., Lack, D., Müller, T., Niessner, R., Petzold, a., Piazzalunga, a., Putaud, J. P., Schwarz, J., Sheridan, P., Subramanian, R., Swietlicki, E., Valli, G., Vecchi, R.

and Viana, M.: Soot reference materials for instrument calibration and intercomparisons: a workshop summary with recommendations, Atmos. Meas. Tech., 5(8), 1869–1887, doi:10.5194/amt-5-1869-2012, 2012.

Bond, T. C. and Bergstrom, R. W.: Light Absorption by Carbonaceous Particles: An Investigative Review, Aerosol Sci. Technol., 40(1), 27–67, doi:10.1080/02786820500421521, 2006.

Bond, T. C., Doherty, S. J., Fahey, D. W., Forster, P. M., Berntsen, T., DeAngelo, B. J., Flanner, M. G., Ghan, S., Kärcher, B., Koch, D., Kinne, S., Kondo, Y., Quinn, P. K., Sarofim, M. C., Schultz, M. G., Schulz, M., Venkataraman, C., Zhang, H., Zhang, S., Bellouin, N., Guttikunda, S. K., Hopke, P. K., Jacobson, M. Z., Kaiser, J. W., Klimont, Z., Lohmann, U., Schwarz, J. P., Shindell, D., Storelvmo, T., Warren, S. G. and Zender, C. S.: Bounding the role of black carbon in the climate system: A scientific assessment, J. Geophys. Res. Atmos., 118(11), 5380–5552, doi:10.1002/jgrd.50171, 2013.

Chang, R. Y.-W., Slowik, J. G., Shantz, N. C., Vlasenko, A., Liggio, J., Sjostedt, S. J., Leaitch, W. R. and Abbatt, J. P. D.: The hygroscopicity parameter (κ) of ambient organic aerosol at a field site subject to biogenic and anthropogenic influences: relationship to degree of aerosol oxidation, Atmos. Chem. Phys., 10(11), 5047–5064, doi:10.5194/acp-10-5047-2010, 2010.

Cooke, W., Jennings, S. G. and Spain, T. G.: Black carbon measurements at Mace Head, 1989–1996, J. Geophys. Res., 102, 1989–1996, doi:10.1029/97JD01430, 1997.

Cozic, J., Verheggen, B., Mertes, S., Connolly, P., Bower, K., Petzold, A., Baltensperger, U. and Weingartner, E.: Scavenging of black carbon in mixed phase clouds at the high alpine site Jungfraujoch, Atmos. Chem. Phys., 7(7), 1797–1807, 2007.

DeCarlo, P. F., Kimmel, J. R., Trimborn, A., J., N. M., Jayne, J. T., Aiken, A. C., Gonin, M., Fuhrer, K., Horvath, T., Docherty, K. S., Worsnop, D. R. and Jimenez, J. L.: Field-deployable, high-resolution, time-of-flight aerosol mass spectrometer, Anal. Chem., 78(24), 8281–8289, doi:10.1021/ac061249n, 2006.

Draxler, R. R. and Rolph, G. D.: HYSPLIT (HYbrid Single-Particle Langrangian Integrated Trajectory) Model access via NOAA ARL READY Website . NOAA Air Resources Laboratory, Silver Spring, MD., [online] Available from: http://ready.arl.noaa.gov/HYSPLIT.php, 2013.

Eugster, W., Burkard, R., Holwerda, F., Scatena, F. N. and Bruijnzeel, L. A. (Sampurno.: Characteristics of fog and fogwater fluxes in a Puerto Rican elfin cloud forest, Agric. For. Meteorol., 139(3), 288–306, 2006.

Fierce, L., Riemer, N. and Bond, T. C.: When is cloud condensation nuclei activity sensitive to particle characteristics at emission?, J. Geophys. Res. Atmos., 118(24), 13,476–13,488, doi:10.1002/2013JD020608, 2013.

Gao, R. S., Schwarz, J. P., Kelly, K. K., Fahey, D. W., Watts, L. a., Thompson, T. L., Spackman, J. R., Slowik, J. G., Cross, E. S., Han, J.-H., Davidovits, P., Onasch, T. B. and Worsnop, D. R.: A Novel Method for Estimating Light-Scattering Properties of Soot Aerosols Using a Modified Single-Particle Soot Photometer, Aerosol Sci. Technol., 41(2), 125–135, doi:10.1080/02786820601118398, 2007.

Gieray, R., Wieser, P., Engelhardt, T., Swietlicki, E., Hansson, H.-C., Mentes, B., Orsini, D., Martinsson, B., Svenningsson, B., Noone, K. J. and Heintzenbergg, J.: PHASE PARTITIONING OF AEROSOL CONSTITUENTS IN CLOUD BASED ON SINGLE-PARTICLE AND BULK ANALYSIS, Atmos. Environ., 31(16), 2491–2502, 1997.

Glantz, P. and Noone, K. J.: A physically-based algorithm for estimating the relationship between aerosol mass and cloud droplet number, Tellus B, 52B, 1216–1231, 2000.

Granat, L., Engström, J. E., Praveen, S. and Rodhe, H.: Light absorbing material (soot) in rainwater and in aerosol particles in the Maldives, J. Geophys. Res., 115(D16307), 1–12, doi:10.1029/2009JD13768, 2010.

Gysel, M. and Crosier, J.: Closure study between chemical composition and hygroscopic growth of aerosol particles during TORCH2, Atmos. Chem. Phys., 7(24), 6131–6144, 2007.

Gysel, M., Laborde, M., Olfert, J. S., Subramanian, R. and Gröhn, A. J.: Effective density of Aquadag and fullerene soot black carbon reference materials used for SP2 calibration, Atmos. Meas. Tech., 4(12), 2851–2858, doi:10.5194/amt-4-2851-2011, 2011.

Hallberg, A., Ogren, J. A., Noone, K. J., Heintzenberg, J., Berner, A., Solly, I., Kruisz, C., Reischl, G., Fuzzi, S., Facchini, M. C., Hansson, H.-C., Wiedensohler, A. and Svenningsson, I. B.: Phase partitioning for different aerosol species in fog, Tellus B, 44B(5), 545–555, 1992.

Hallberg, A., Ogren, J. A., Noone, K. J., Okada, K., Heintzenberg, J. and Svenningsson, I. B.: The influence of aerosol particle composition on cloud droplet formation, J. Atmos. Chem., 19, 153–171, 1994.

Hawkins, L. N., Russell, L. M., Covert, D. S., Quinn, P. K. and Bates, T. S.: Carboxylic acids, sulfates, and organosulfates in processed continental organic aerosol over the southeast Pacific Ocean during VOCALS-REx 2008, J. Geophys. Res., 115(D13201), doi:10.1029/2009JD013276, 2010.

Hersey, S. P., Craven, J. S., Metcalf, A. R., Lin, J., Lathem, T., Suski, K. J., Cahill, J. F., Duong, H. T., Sorooshian, A., Jonsson, H. H., Shiraiwa, M., Zuend, A., Nenes, A., Prather, K. A., Flagan, R. C. and Seinfeld, J. H.: Composition and hygroscopicity of the Los Angeles Aerosol: CalNex, J. Geophys. Res. Atmos., 118(7), 3016–3036, doi:10.1002/jgrd.50307, 2013.

Hitzenberger, R., Berner, A., Glebl, H., Drobesch, K., Kasper-Giebl, A., Loeflund, M., Urban, H. and Puxbaum, H.: Black carbon (BC) in alpine aerosols and cloud water - concentrations and scavenging efficiencies, Atmos. Environ., 35(30), 5135–5141, 2001.

Hitzenberger, R., Berner, A., Kromp, R., Kasper-Giebl, A., Limbeck, A., Tscherwenka, W. and Puxbaum, H.: Black carbon and other species at a high-elevation European site (Mount Sonnblick, 3106 m, Austria): Concentrations and scavenging efficiencies, J. Geophys. Res., 105(D20), 24637–24645, 2000.

Kasper-Giebl, A., Koch, A., Hitzenberger, R. and Puxbaum, H.: Scavenging efficiency of "aerosol carbon"and sulfate in supercooled clouds at Mt. Sonnblick (3106 m asl, Austria), J. Atmos. Chem., 35, 33–46, 2000.

Laborde, M., Mertes, P., Zieger, P., Dommen, J., Baltensperger, U. and Gysel, M.: Sensitivity of the Single Particle Soot Photometer to different black carbon types, Atmos. Meas. Tech., 5(5), 1031–1043, doi:10.5194/amt-5-1031-2012, 2012.

Lance, S., Raatikainen, T., Onasch, T. B., Worsnop, D. R., Yu, X.-Y., Alexander, M. L., Stolzenburg, M. R., McMurry, P. H., Smith, J. N. and Nenes, A.: Aerosol mixing state, hygroscopic growth and cloud activation efficiency during MIRAGE 2006, Atmos. Chem. Phys., 13(9), 5049–5062, doi:10.5194/acp-13-5049-2013, 2013.

Lathem, T. L., Beyersdorf, A. J., Thornhill, K. L., Winstead, E. L., Cubison, M. J., Hecobian, A., Jimenez, J. L., Weber, R. J., Anderson, B. E. and Nenes, A.: Analysis of CCN activity of Arctic aerosol and Canadian biomass burning during summer 2008, Atmos. Chem. Phys., 13(5), 2735–2756, doi:10.5194/acp-13-2735-2013, 2013.

Lide, D. R., Ed.: CRC Handbook of Chemistry and Physics, 82nd ed., CRC Press., 2001.

Mätzler, C.: MATLAB Functions for Mie Scattering and Absorption Version 1 - Research Report No. 2002-08, [online] Available from: http://www.iap.unibe.ch/publications/download/201/en/, 2002a.

Mätzler, C.: MATLAB Functions for Mie Scattering and Absorption Version 2 - Research Report No. 2002-11, [online] Available from: www.iap.unibe.ch/publications/download/199/en/, 2002b.

Mei, F., Hayes, P. L., Ortega, A., Taylor, J. W., Allan, J. D., Gilman, J., Kuster, W., de Gouw, J., Jimenez, J. L. and Wang, J.: Droplet activation properties of organic aerosols observed at an urban site during CalNex-LA, J. Geophys. Res. Atmos., 118(7), 2903–2917, doi:10.1002/jgrd.50285, 2013.

Metcalf, A. R., Craven, J. S., Ensberg, J. J., Brioude, J., Angevine, W., Sorooshian, A., Duong, H. T., Jonsson, H. H., Flagan, R. C. and Seinfeld, J. H.: Black carbon aerosol over the Los Angeles Basin during CalNex, J. Geophys. Res. Atmos., 117(D00V13), 1–24, doi:10.1029/2011JD17255, 2012.

Moore, R. H., Cerully, K., Bahreini, R., Brock, C. A., Middlebrook, A. M. and Nenes, A.: Hygroscopicity and composition of California CCN during summer 2010, J. Geophys. Res. Atmos., 117(D00V12), 1–14, doi:10.1029/2011JD017352, 2012.

Moteki, N. and Kondo, Y.: Effects of Mixing State on Black Carbon Measurements by Laser-Induced Incandescence, Aerosol Sci. Technol., 41(4), 398–417, doi:10.1080/02786820701199728, 2007.

Moteki, N., Kondo, Y. and Nakamura, S.: Method to measure refractive indices of small nonspherical particles: Application to black carbon particles, J. Aerosol Sci., 41(5), 513–521, doi:10.1016/j.jaerosci.2010.02.013, 2010.

Moteki, N., Kondo, Y., Takegawa, N. and Nakamura, S.: Directional dependence of thermal emission from nonspherical carbon particles, J. Aerosol Sci., 40(9), 790–801, doi:10.1016/j.jaerosci.2009.05.003, 2009.

Noone, K. J., Ogren, J. a., Heintzenberg, J., Charlson, R. J. and Covert, D. S.: Design and Calibration of a Counterflow Virtual Impactor for Sampling of Atmospheric Fog and Cloud Droplets, Aerosol Sci. Technol., 8(3), 235–244, 1988.

O'Dowd, C., Becker, E. and Kulmala, M.: Mid-latitude North-Atlantic aerosol characteristics in clean and polluted air, Atmos. Res., 58(3), 167–185, 2001.

Ovadnevaite, J., Ceburnis, D., Canagaratna, M., Berresheim, H., Bialek, J., Martucci, G., Worsnop, D. R. and O'Dowd, C.: On the effect of wind speed on submicron sea salt mass concentrations and source fluxes, J. Geophys. Res., 117(D16201), 1–11, doi:10.1029/2011JD017379, 2012.

Pekour, M. S. and Cziczo, D. J.: Wake capture, particle breakup, and other artifacts associated with counterflow virtual impaction, Aerosol Sci. Technol., 45, 758–764, doi:10.1080/02786826.2011.558942, 2011.

Petters, M. D. and Kreidenweis, S. M.: A single parameter representation of hygroscopic growth and cloud condensation nucleus activity, Atmos. Chem. Phys., 7(8), 1961–1971, 2007.

Pirjola, L. and O'Dowd, C.: Can new particle formation occur in the clean marine boundary layer?, J. Geophys. Res., 105(D21), 26531–26546, 2000.

Pratt, K. a., Heymsfield, A. J., Twohy, C. H., Murphy, S. M., DeMott, P. J., Hudson, J. G., Subramanian, R., Wang, Z., Seinfeld, J. H. and Prather, K. a.: In Situ Chemical Characterization of Aged Biomass-Burning Aerosols Impacting Cold Wave Clouds, J. Atmos. Sci., 67(8), 2451–2468, doi:10.1175/2010JAS3330.1, 2010.

Riemer, N., West, M., Zaveri, R. and Easter, R.: Estimating black carbon aging time-scales with a particle-resolved aerosol model, J. Aerosol Sci., 41(1), 143–158, doi:10.1016/j.jaerosci.2009.08.009, 2010.

Rolph, G. D.: Real-time Environmental Application and Display sYstem (READY) Website. NOAA Air Resources Laboratory, Silver Spring, MD., [online] Available from: http//ready.arl.noaa.gov, 2013.

Rose, D., Gunthe, S. S., Mikhailov, E., Frank, G. P., Dusek, U., Andreae, M. O. and Pöschl, U.: Calibration and measurement uncertainties of a continuous-flow cloud condensation nuclei counter (DMT-CCNC): CCN activation of ammonium sulfate and sodium chloride aerosol particles in theory and experiment, Atmos. Chem. Phys., 8(5), 1153–1179, 2008.

Rose, D., Nowak, A., Achtert, P., Wiedensohler, A., Hu, M., Shao, M., Zhang, Y., Andreae, M. O. and Pöschl, U.: Cloud condensation nuclei in polluted air and biomass burning smoke near the mega-city Guangzhou, China – Part 1: Size-resolved measurements and implications for the modeling of aerosol particle hygroscopicity and CCN activity, Atmos. Chem. Phys., 10(7), 3365–3383, 2010.

Schwarz, J. P., Gao, R. S., Fahey, D. W., Thomson, D. S., Watts, L. A., Wilson, J. C., Reeves, J. M., Darbeheshti, M., Baumgardner, D. G., Kok, G. L., Chung, S. H., Schulz, M., Hendricks, J., Lauer, A., Kärcher, B., Slowik, J. G., Rosenlof, K. H., Thompson, T. L., Langford, a. O., Loewenstein, M. and Aikin, K. C.: Single-particle measurements of midlatitude black carbon and light-scattering aerosols from the boundary layer to the lower stratosphere, J. Geophys. Res., 111(D16207), 1–15, doi:10.1029/2006JD007076, 2006.

Schwarz, J. P., Gao, R. S., Spackman, J. R., Watts, L. A., Thomson, D. S., Fahey, D. W., Ryerson, T. B., Peischl, J., Holloway, J. S., Trainer, M., Frost, G. J., Baynard, T., Lack, D. a., de Gouw, J. a., Warneke, C. and Del Negro, L. a.: Measurement of the mixing state, mass, and optical size of individual black carbon particles in urban and biomass burning emissions, Geophys. Res. Lett., 35(13), L13810, doi:10.1029/2008GL033968, 2008a.

Schwarz, J. P., Spackman, J. R., Fahey, D. W., Gao, R. S., Lohmann, U., Stier, P., Watts, L. a., Thomson, D. S., Lack, D. A., Pfister, L., Mahoney, M. J., Baumgardner, D., Wilson, J. C. and Reeves, J. M.: Coatings and their enhancement of black carbon light absorption in the tropical atmosphere, J. Geophys. Res., 113(D03203), 1–10, doi:10.1029/2007JD009042, 2008b.

Schwarz, J. P., Spackman, J. R., Gao, R. S., Perring, a. E., Cross, E., Onasch, T. B., Ahern, A., Wrobel, W., Davidovits, P., Olfert, J., Dubey, M. K., Mazzoleni, C. and Fahey, D. W.: The Detection Efficiency of the Single Particle Soot Photometer, Aerosol Sci. Technol., 44(8), 612–628, doi:10.1080/02786826.2010.481298, 2010.

Schwarzenboeck, A.: CUT SIZE MINIMIZATION AND CLOUD ELEMENT BREAK-UP IN A GROUND-BASED CVI, , 31(4), 477–489, 2000.

Sedlacek, A. J., Lewis, E. R., Kleinman, L., Xu, J. and Zhang, Q.: Determination of and evidence for non-core-shell structure of particles containing black carbon using the Single-Particle Soot Photometer (SP2), Geophys. Res. Lett., 39(6), L06802, doi:10.1029/2012GL050905, 2012.

Sellegri, K., Laj, P., Dupuy, R., Legrand, M., Preunkert, S. and Putaud, J.-P.: Size-dependent scavenging efficiencies of multicomponent atmospheric aerosols in clouds, J. Geophys. Res., 108(D11), 4334, doi:10.1029/2002JD002749, 2003.

Shank, L. M., Howell, S., Clarke, A. D., Freitag, S., Brekhovskikh, V., Kapustin, V., McNaughton, C., Campos, T. and Wood, R.: Organic matter and non-refractory aerosol over the remote Southeast Pacific: oceanic and combustion sources, Atmos. Chem. Phys., 12(1), 557–576, doi:10.5194/ACP-12-557-2012, 2012.

Shantz, N. C., Leaitch, W. R., Phinney, L., Mozurkewich, M. and Toom-Sauntry, D.: The effect of organic compounds on the growth rate of cloud droplets in marine and forest settings, Atmos. Chem. Phys., 8(19), 5869–5887, 2008.

Spiegel, J. K., Zieger, P., Bukowiecki, N., Hammer, E., Weingartner, E. and Eugster, W.: Evaluating the capabilities and uncertainties of droplet measurements for the fog droplet spectrometer (FM-100), Atmos. Meas. Tech., 5(9), 2237–2260, doi:10.5194/amt-5-2237-2012, 2012.

Stephens, M., Turner, N. and Sandberg, J.: Particle identification by laser-induced incandescence in a solid-state laser cavity., Appl. Opt., 42(19), 3726–3736, 2003.

Subramanian, R., Kok, G. L., Baumgardner, D., Clarke, A., Shinozuka, Y., Camps, T. L., Hizer, C. G., Stephens, B. B., de Foy, P. B. and Zaveri, R. A.: Black carbon over Mexico: the effect of atmospheric transport on mixing state, mass absorption cross-section, and BC/CO ratios, Atmos. Chem. Phys., 10(1), 219–237 [online] Available from: http://www.atmos-chem-phys.net/10/219/2010/ (Accessed 16 November 2014), 2010.

Targino, A. C., Noone, K. J., Drewnick, F., Schneider, J., Krejci, R., Olivares, G., Hings, S. and Borrmann, S.: Microphysical and chemical characteristics of cloud droplet residuals and interstitial particles in continental stratocumulus clouds, Atmos. Res., 86(3-4), 225–240, doi:10.1016/j.atmosres.2007.05.001, 2007.

Taylor, J. W., Allan, J. D., Liu, D., Flynn, M., Weber, R., Zhang, X., Lefer, B. L., Grossberg, N., Flynn, J. and Coe, H.: Assessment of the sensitivity of core/shell parameters derived using the single-particle soot photometer to density and refractive index, Atmos. Meas. Tech. Discuss., 7(6), 5491–5532, doi:10.5194/amtd-7-5491-2014, 2014.

Twohy, C. H., Petters, M. D., Snider, J. R., Stevens, B., Tahnk, W., Wetzel, M., Russell, L. M. and Burnet, F.: Evaluation of the aerosol indirect effect in marine stratocumulus clouds: Droplet number, size, liquid water path, and radiative impact, J. Geophys. Res., 110, 1–16, doi:10.1029/2004JD005116, 2005.

Vidaurre, G., Hallett, J. and Rogers, D. C.: Airborne Measurement of Liquid and Total Water Content, J. Atmos. Ocean. Technol., 28(9), 1088–1103, 2011.

Wang, J., Lee, Y.-N., Daum, P. H., Jayne, J. and Alexander, M. L.: Effects of aerosol organics on cloud condensation nucleus (CCN) concentration and first indirect aerosol effect, Atmos. Chem. Phys., 8(21), 6325–6339 [online] Available from: www.atmos-chem-phys.net/8/6325/2008/ (Accessed 16 November 2014), 2008.

Wang, Q., Jacob, D. J., Spackman, J. R., Perring, A. E., Schwarz, J. P., Moteki, N., Marais, E. a., Ge, C., Wang, J. and Barrett, S. R. H.: Global budget and radiative forcing of black carbon aerosol: Constraints from pole-to-pole (HIPPO) observations across the Pacific, J. Geophys. Res. Atmos., 119(1), 195–206, doi:10.1002/2013JD020824, 2014.

Von der Weiden, S.-L., Drewnick, F. and Borrmann, S.: Particle Loss Calculator – a new software tool for the assessment of the performance of aerosol inlet systems, Atmos. Meas. Tech., 2(2), 479–494, 2009.

Wu, Z. J., Poulain, L., Henning, S., Dieckmann, K., Birmili, W., Merkel, M., van Pinxteren, D., Spindler, G., Müller, K., Stratmann, F., Herrmann, H. and Wiedensohler, A.: Relating particle hygroscopicity and CCN activity to chemical composition during the HCCT-2010 field campaign, Atmos. Chem. Phys., 13(16), 7983–7996, doi:10.5194/acp-13-7983-2013, 2013.

Zhao, R., Lee, A. K. K., Liggio, J., Wentzall, J. J. B., Macdonald, A. M., Toom-Sauntry, D., Leaitch, W. R., Modini, R. L., Corrigan, A. L., Russell, L. M., Noone, K. J., Schroder, J. C., Bertram, A. K., Hawkins, L. N. and Abbatt, J. P. D.: Cloud Scavenging of Isocyanic Acid (HNCO) and Evidence of a Secondary Source of HNCO in Ambient Air, Geophys. Res. Lett., Submitted, 2014.